EVALUATION OF PARAMETERS IN A TWO SLAB REACTOR BY RANDOM NOISE MEASUREMENTS

By

ALLEN ROSS BOYNTON

A DISSERTATION PRESENTED TO THE GRADUATE COUNCIL OF
THE UNIVERSITY OF FLORIDA
IN PARTIAL FULFILLMENT OF THE REQUIREMENTS FOR THE
DEGREE OF DOCTOR OF PHILOSOPHY

UNIVERSITY OF FLORIDA
December 1962

ACKNOWLEDGMENTS

The author wishes to acknowledge his gratitude for the advice and encouragement of his advisory committee. In particular, grateful acknowledgment is made to the chairman, Dr. Robert E. Uhrig, for his continued guidance and encouragement during the course of this work.

The author wishes to express his gratitude to the staff and technicians of the Department of Nuclear Engineering. J. Mueller and K. L. Fawcett constructed the early equipment, J. Wildt constructed the final equipment, and L. D. Butterfield operated the reactor for most of the runs.

The author wishes also to express his appreciation to Dr. Herbert Kouts and V. Rajagopal of the Brookhaven National Laboratory for their loan of the random reactivity input device.

TABLE OF CONTENTS

Page

ACKNOWLEDGMENTS ii

LIST OF TABLES iv

LIST OF FIGURES v

Chapter

I. INTRODUCTION 1

II. THEORY 8

- Cross-Power Spectra . . . 9
- Two Region Transfer Functions . . . 20
- Reduction of Equations . . . 31

III. MEASURING SYSTEM 38

- Measuring Theory . . . 38
- The University of Florida Training Reactor . . . 44
- Cross-Power Spectrum Analyzer . . . 47
- Random Reactivity Input Device . . . 60

IV. EXPERIMENTS AND RESULTS 65

- Calibration . . . 65
- Reactor Data . . . 82

V. DISCUSSION AND CONCLUSIONS 103

Appendix

A. CALCULATION OF TRANSIT TIME BETWEEN SLABS 108

B PHASE SHIFT AND HIGH PASS FILTER DETAILS 113

C. OPERATION OF CROSS-POWER SPECTRUM ANALYZER 119

LIST OF REFERENCES 123

BIOGRAPHICAL SKETCH 126

LIST OF TABLES

Table		Page
1.	Results of Run L	69
2.	Results of Run M	70
3.	Results of Run P	73
4.	Results of Run R	83
5.	Results of Run CC	90
6.	Results of Run Z	95
7.	Results of Run Q	101
8.	Value of Transit Time Between Slabs	111
9.	Set Points for Phase Shifters	116
10.	Correction Factors for Filters	118

LIST OF FIGURES

Figure		Page
1.	Two Region System Diagram	10
2.	Normalized Amplitude Component of $R_{12}(\omega)$ for Several Values of B . . .	35
3.	Phase Component of $R_{12}(\omega)_{\theta}$ for Several Values of B and θ	36
4.	Sequence of Operations Necessary for Experimental Determination of Power Spectrum	42
5	Sequence of Operations Necessary for Experimental Determination of Cross-Power Spectrum	42
6	Location of Ion Chambers in UFTR Core .	46
7	Data Transcribing System	48
8.	Modulator Schematic	50
9	Cross-Power Spectrum Analyzer	52
10.	Demodulator Schematic	53
11	Random Reactivity Input Device	61
12.	Power Amplifier Schematic	63
13.	Normalized Amplitude Component of $G(\omega)$ from Runs L and M	71
14	Phase Component of $G(\omega)$ from Runs L and M	72
15.	Normalized Power Spectrum of Random Step from Run L	73

LIST OF FIGURES (Cont'd)

Figure Page

16. Normalized Amplitude Component of $G(\omega)$ from Run P 80

17. Phase Component of $G(\omega)$ from Run P . . 81

18. Normalized Amplitude Component of $R_{12}(\omega)$ from Run R 85

19 Phase Component of $R_{12}(\omega)$ from Run R . 86

20. Normalized Power Spectrum of Region 1 Output from Run R 87

21. Normalized Amplitude Component of $R_{12}(\omega)$ from Run CC 91

22. Phase Component of $R_{12}(\omega)$ from Run CC . 92

23. Normalized Power Spectrum of Region 1 Output from Run CC 93

24. Amplitude Component of Normalized Cross-Power Spectrum from Run Z 96

25. Phase Component of Normalized Cross-Power Spectrum from Run Z 97

26. Normalized Power Spectrum of Region 1 Output from Run Z 98

27. Normalized Power Spectrum of Region 1 Output from Run Q 102

CHAPTER I

INTRODUCTION

This study is a development of an experimental method to measure the parameters peculiar to a two region reactor system. Of particular interest is the method of representing the coupling or interaction between the two regions. A transfer function approach is used.

The dynamic behavior of reactors has been successfully analyzed from the transfer function point of view. Transfer functions have been instrumental in determining system stability and the design of control systems. The measurement of reactor transfer functions by sinusoidal oscillations, step, and ramp inputs of reactivity are standard techniques and have allowed the determination of parameters associated with the reactor kinetics equations (1) (2).*

However, the statistical nature of the fission process has led many investigators to measure dynamic reactor parameters by purely statistical means. As early as 1946, deHoffman (3) developed an expression for the intensity fluctuations of a chain reactor as measured by a counter with statistical response. The formulation included the effects of delayed neutrons and involved the dispersion of the number of neutrons emitted per fission. Later workers in this area were Luckow (4) who used the variance to mean ratio of the number of neutrons counted by a detector during a fixed counting time to measure the prompt neutron lifetime; Albrecht (5) who extended Luckow's analysis to include delayed neutron parameters; and Valez (6) who used the autocorrelation function of the counting rate from a reactor to measure the dynamic parameters. These investigations, while giving insight into the fundamental nature of multiplying systems and information on the influence of the statistical fluctuations in the reactor power level on such things as the precision of neutron measurements and the design of reactor control equipment, cannot furnish as much information about the complete reactor system as can the transfer function.

---

*Underlined numbers in parentheses refer to the list of references.

Fortunately, statistical considerations are related to the transfer function approach, since the power spectral density functions (or power spectra) and correlation functions form a Fourier transform pair. Correlation functions have been known to statisticians for many years, yet were relatively unknown to engineers, who were analyzing frequencies and power spectra. Since the power spectrum is related to the transfer function of a linear system, engineers have been quick to use this new measuring technique.

Moore (7) (8) was among the first to relate the statistical nature of chain reactors to their transfer functions when he expressed the power spectrum of the reactor noise as a function of the square of the modulus of the transfer function. Cohn (9) used a band pass filter to measure the high frequency portion of the reactor noise spectrum which is dependent on the ratio of the effective delayed neutron fraction, β, to the prompt neutron lifetime, ℓ. This technique has become almost standard (10). The method has, however, several difficulties. First, the exact input to the system is not definable. This difficulty is attacked by Cohn (11) who assumes the reactor noise to arise from a random "noise equivalent" neutron source driving the reactor. The characteristics of this source are calculated from conventional random noise theory, and the resulting pile noise obtained through the use of the source transfer function. Bennett (12) develops the spectrum and variance of pile noise according to the formulation of Rice (13). Recent measurements (14) have indicated that the inherent reactor driving function spectrum deviates from white noise at low frequencies. Second, the effects of external disturbances on the final result are uncertain since the measured noise is actually a combination of reactor fluctuations and instrument noise. Third, the autocorrelation or pile noise spectrum method does not yield any direct information about the phase of the transfer function. A fourth objection to this method is that a large (greater than $5x10^{-4}$) detector efficiency is required. It may be physically impossible to place a detector in a position of high efficiency, and in the case of a counting experiment, the power level may need to be limited to avoid pile-up in the detector.

These objections are removed by crosscorrelation techniques. Balcomb (15) and Rajagopal (16) investigated the crosscorrelation of reactor outputs with random reactivity inputs. Both these investigators measured unit impulse response functions and then found the transfer function by taking the Fourier transform. It was found that the technique is very effective in eliminating the effects of external noise and gave good results for low-level crosscorrelation signal inputs whose power was comparable to the noise power in the system.

This paper will apply this latest technique to a more complex reactor model, that of a two region reactor.

Baldwin (17) has examined the so-called "two-slab" loading of the Argonaut reactor and found that, experimentally, a single exponential stable period is observed when the system is supercritical, but that there is a tendency for independent behavior of the two slabs, resulting in so-called "flux tilting." Rod calibration experiments, indicated that the ratio of fluxes in the two fuel regions changes during the calibration procedure. It was also found that the single transfer function of a simple reactor system was inadequate to treat the two slab system.

The two (or more) region reactor has also been of interest in connection with the phenomenon of coupled Xenon oscillations in large reactors (18).

The University of Florida Training Reactor (UFTR) is a two region coupled reactor. Each fuel region is subcritical when considered separately, but coupling between the two regions allows the system to become critical. If the multiplication factor of one region is disturbed, the other region will be disturbed only through its coupling to the first. A study of the interdependence of the outputs of the two regions, when an external disturbance is given to only one of them, will reveal something about the nature of the coupling between the two regions. A representation of this interdependence is given by either the crosscorrelation function of the outputs of the two regions, or in the frequency domain, by the cross-power spectrum between the two outputs.

The relations for the cross-power spectra between the outputs of each region are derived and are found to involve transfer functions of the individual regions. When these transfer functions are derived, they are found to depart from the conventional one region transfer functions because of the term that couples the two regions. The cross-power spectrum between the outputs of the two regions is a complex quantity and its phase part is found to be sensitive to the transit time of a disturbance between the regions. Its amplitude part as well as the phase part is found to be dependent on the value of the multiplication factor of the undisturbed region.

The cross-power spectrum between the outputs of both regions of the UFTR was measured under two conditions: (a) a random stationary external input to region 1, and (b) no external input to either region.

Continuous data from two ion chambers were amplitude modulated and stored on magnetic tape. The cross-power spectra were then measured directly using band pass filters and an analog computer.

These data from the UFTR indicate that the propagation of a disturbance in one region of the reactor to the other region may adequately be described in terms of neutron waves. Also shown is the feasibility of measuring the multiplication factor of each side and the magnitude of the coupling between the two regions.

CHAPTER II

THEORY

The experiment to be analyzed consists of measuring the cross-power spectrum of the outputs of each region of a two region reactor. These outputs are examined under two operational conditions: (a) a random stationary external input to region 1 and, (b) no external input to either region. These cross-power spectra are then related to the transfer functions of the individual regions.

In the first section of this chapter, the relations that involve the two coupled linear systems and their inputs and outputs are developed. Although these relations are general in nature and not restricted to reactor systems, they are developed so as to be directly applicable to the experiment. This is evidenced by the transformation of the relations from the time domain into the frequency domain so that the linear systems involved are represented by their transfer functions.

In the second section, these transfer functions are developed from the reactor kinetics equations that are derived for a two slab coupled reactor system.

The final section brings the cross-power spectra and transfer functions together. After certain simplifying assumptions are made, the equations are examined for the measurement of the parameters particular to the two slab reactor system.

Cross-Power Spectra

Consider a two region coupled system as shown in Figure 1. Each region is a linear system having its own unit impulse response function $h_1(t)$ and $h_2(t)$, and outputs given by $f_1(t)$ and $f_2(t)$. The regions are coupled to one another because a certain fraction, k_1, of the output of region 1 is received as an input to region 2 after a transit time θ, and vice versa. Region 1 is also subjected to a random stationary external input, $i(t)$.

The crosscorrelation function of the outputs of region 1 and region 2, $\phi_{12}(\tau)$, is defined as (19),

$$\phi_{12}(\tau) = \lim_{T \to \infty} \frac{1}{2T} \int_{-T}^{T} f_1(t) f_2(t+\tau)\,dt\,, \qquad (1)$$

where τ is a continuous displacement time independent of t. The two systems have been specified to be linear,

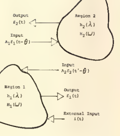

Figure 1. Two Region System Diagram

so the convolution integral between the input, output, and unit impulse response function is given as (19),

$$f_1(t) = \int_{-\infty}^{\infty} h_1(\lambda)\ \mathrm{Input}(t-\lambda)\,d\lambda \ . \qquad (2)$$

Reference to Figure 1 shows that the input to region 1 is the sum of the external input, i(t), and the fraction, A_2, of the output of region 2, at a previous time corresponding to the transit time, θ, between the regions. Thus,

$$\mathrm{Input}(t) = i(t) + A_2 f_2(t - \theta) \ . \qquad (3)$$

Equation (2) is now written as

$$f_1(t) = \int_{-\infty}^{\infty} h_1(\lambda) \left[i(t-\lambda) + A_2 f_2(t-\lambda-\theta) \right] d\lambda , \qquad (4)$$

which may be substituted into the definition of the crosscorrelation function between the outputs of region 1 and region 2, equation (1), to give

$$\phi_{12}(\tau) = \lim_{T \to \infty} \frac{1}{2T} \int_{-T}^{T} \int_{-\infty}^{\infty} h_1(\lambda) \left[i(t-\lambda) + A_2 f_2(t-\lambda-\theta) \right] d\lambda\, f_2(t+\tau)\,dt . \qquad (5)$$

By reversing the order of integration, equation (5) is put into a more desirable form,

$$\phi_{12}(\tau) = \int_{-\infty}^{\infty} h_1(\lambda) \lim_{T\rightarrow\infty} \frac{1}{2T} \int_{-T}^{T} i(t-\lambda) f_2(t+\tau)\,dt\,d\lambda$$

$$+ A_2 \int_{-\infty}^{\infty} h_1(\lambda) \lim_{T\rightarrow\infty} \frac{1}{2T} \int_{-T}^{T} f_2(t-\lambda-\theta) f_2(t+\tau)\,dt\,d\lambda . \tag{6}$$

With this grouping, the inner integral in the first term is recognized as the crosscorrelation function between the external input and the output of region 2, while the inner integral in the second term is the autocorrelation function of the region 2 output. Equation (6) may now be written in the compact form,

$$\phi_{12}(\tau) = \int_{-\infty}^{\infty} h_1(\lambda) \phi_{12}(\tau+\lambda)\,d\lambda$$

$$+ A_2 \int_{-\infty}^{\infty} h_1(\lambda) \phi_{22}(\tau+\lambda+\theta)\,d\lambda . \tag{7}$$

From equation (1), it is noticed that $f_2(t+\tau)$ may also be expressed in terms of the convolution integral between the input, output, and unit impulse response function by,

$$f_2(t) = \int_{-\infty}^{\infty} h_2(\lambda)\,\text{Input}(t-\lambda)\,d\lambda . \qquad (8)$$

In region 2 the only input is that fraction, A_1, of the output of region 1 which reaches region 2 after the transit time, θ, between the regions. Thus,

$$\text{Input}(t) = A_1 f_1(t-\theta). \qquad (9)$$

Equation (8) is written as

$$f_2(t) = A_1\int_{-\infty}^{\infty} h_2(\lambda) f_1(t-\lambda-\theta)\,d\lambda , \qquad (10)$$

which, when substituted into equation (1), gives,

$$\phi_{12}(\tau) = \lim_{T\to\infty}\frac{1}{2T}\int_{-T}^{T} f_1(t) A_1 \int_{-\infty}^{\infty} h_2(\lambda) f_1(t+\tau-\lambda-\theta)\,d\lambda\,dt. \qquad (11)$$

Once again, inversion of the order of integration will yield a more convenient grouping,

$$\phi_{12}(\tau) = A_1\int_{-\infty}^{\infty} h_2(\lambda) \lim_{T\to\infty}\frac{1}{2T}\int_{-T}^{T} f_1(t) f_1(t+\tau-\lambda-\theta)\,dt\,d\lambda , \qquad (12)$$

in which the inner integral is recognized as the autocorrelation function of the output of region 1. Equation (12) can now be written in a more compact form, and with equation (7) relates the crosscorrelation of the outputs of region 1 and region 2 with their unit impulse response functions, their autocorrelation functions, and the crosscorrelation of the external input and the output of region 2.

$$\phi_{12}(\tau) = A_1\int_{-\infty}^{\infty} h_2(\lambda)\phi_{11}(\tau-\lambda-\theta)d\lambda . \quad (13)$$

An obvious simplification is the case of no external input to the two region system Equation (13) is unchanged, but equation (7) becomes,

$$\phi_{12}(\tau) = A_2\int_{-\infty}^{\infty} h_1(\lambda)\phi_{22}(\tau+\lambda+\theta)d\lambda . \quad (14)$$

These relations may now be transformed into the frequency domain by taking the Fourier transform of both sides of both equations. As previously noted this is done to relate the theory directly with the experiment. Many investigators (16) (17) choose to measure crosscorrelation and autocorrelation functions (rather than the cross-power and power spectra) of the outputs and obtain unit impulse response functions. The Fourier transformation of the unit impulse response function which gives the transfer function, is performed on a digital computer. If the cross-power and power spectra can be measured directly, a computer operation may be eliminated. The equipment available to the author also suggested the direct measurement of the cross-power and power spectra. Equations (7) and (13) must then be examined in the frequency domain.

The Fourier transform of equation (7) is taken by multiplying both sides of the equation by $\frac{1}{2\pi}e^{-j\omega\tau}$, where $j = \sqrt{-1}$, ω is the angular frequency (radians per second), and integrating with respect to τ. Equation (7) then becomes,

$$\frac{1}{2\pi}\int_{-\infty}^{\infty}\phi_{12}(\tau)e^{-j\omega\tau}d\tau$$

$$= \frac{1}{2\pi}\int_{-\infty}^{\infty}e^{-j\omega\tau}d\tau\int_{-\infty}^{\infty}h_1(\lambda)\phi_{12}(\tau+\lambda)d\lambda$$

$$+ \frac{A_2}{2\pi}\int_{-\infty}^{\infty}e^{-j\omega\tau}d\tau\int_{-\infty}^{\infty}h_1(\lambda)\phi_{22}(\tau+\lambda+\theta)d\lambda . \tag{15}$$

The crosscorrelation function and the cross-power spectrum are a Fourier transform pair defined by (20),

$$\Phi_{12}(\omega) = \frac{1}{2\pi}\int_{-\infty}^{\infty} \phi_{12}(\tau)e^{-j\omega\tau}\,d\tau \quad \text{and} \qquad (16)$$

$$\phi_{12}(\tau) = \int_{-\infty}^{\infty} \Phi_{12}(\omega)e^{j\omega\tau}\,d\omega \,. \qquad (17)$$

The term on the left side of equation (15) is then by definition the cross-power spectrum between the outputs of region 1 and region 2, $\Phi_{12}(\omega)$. In the first double integral on the right side of equation (15), the change of variable,

$$x = \tau + \lambda \,. \qquad (18)$$

is made so that the integral becomes

$$\frac{1}{2\pi}\int_{-\infty}^{\infty} e^{-j\omega(x-\lambda)}dx\int_{-\infty}^{\infty} h_1(\lambda)\phi_{12}(x)\,d\lambda \,. \qquad (19)$$

In this double integral, a separation of variables puts all terms involving x under one integral and all terms involving λ under another. Equation (19) becomes a product of two single integrals,

$$\left[\int_{-\infty}^{\infty} e^{j\omega\lambda}h_1(\lambda)\,d\lambda\right]\left[\frac{1}{2\pi}\int_{-\infty}^{\infty} \phi_{12}(x)e^{-j\omega x}\,dx\right]. \qquad (20)$$

The unit impulse response function and the transfer function are also a Fourier transform pair given by (13),

$$h(t) = \frac{1}{2\pi}\int_{-\infty}^{\infty} H(\omega)e^{j\omega t}\,d\omega \quad \text{and} \tag{21}$$

$$H(\omega) = \int_{-\infty}^{\infty} h(t)e^{-j\omega t}\,dt\ , \tag{22}$$

where $H(\omega)$ is the system transfer function. The first factor in equation (20) is then recognized as the complex conjugate of the transfer function of region 1, $H_1^*(\omega)$. From equation (16), the second factor is identified as the cross-power spectrum between the external input and the output of region 2. In the second and last term on the right of equation (15) the change of variable

$$y = \tau + \lambda + \theta\ , \tag{23}$$

allows a separation of variables as in the first integral which will give a product of two single integrals,

$$A_2 e^{j\omega\theta}\left[\int_{-\infty}^{\infty} h_1(\lambda)e^{j\omega\lambda}\,d\lambda\right]\left[\frac{1}{2\pi}\int_{-\infty}^{\infty}\Phi_{22}(y)e^{-j\omega y}dy\right]. \tag{24}$$

Here, the first factor in brackets is the complex conjugate of the transfer function in region 1, and the second factor in brackets is the power spectrum of the region 2 output. Thus equation (15) may finally be written,

$$\Phi_{12}(\omega) = H_1^*(\omega)\Phi_{12}(\omega) + A_2 e^{j\omega\theta} H_1^*(\omega)\Phi_{22}(\omega). \qquad (25)$$

Equation (13) may be manipulated in the same manner as was equation (7). Taking the Fourier transform of both sides of equation (13) gives,

$$\frac{1}{2\pi}\int_{-\infty}^{\infty}\phi_{12}(\tau)e^{-j\omega\tau}\,d\tau$$

$$= \frac{A_1}{2\pi}\int_{-\infty}^{\infty}e^{-j\omega\tau}\,d\tau\int_{-\infty}^{\infty}h_2(\lambda)\phi_{11}(\tau-\lambda-\theta)\,d\lambda. \qquad (26)$$

A change of variable on the right-hand side of equation (26) to

$$z = \tau - \lambda - \theta \qquad (27)$$

will give, after a separation of variables,

$$\frac{1}{2\pi}\int_{-\infty}^{\infty}\phi_{12}(\tau)e^{-j\omega\tau}\,d\tau$$

$$= A_1 e^{-j\omega\theta}\left[\int_{-\infty}^{\infty}h_2(\lambda)e^{-j\omega\lambda}\,d\lambda\right]\left[\frac{1}{2\pi}\int_{-\infty}^{\infty}\phi_{11}(z)e^{-j\omega z}\,dz\right]. \qquad (28)$$

The left-hand side of equation (28) is recognized as the cross-power spectrum between the outputs of region 1 and region 2, $\Phi_{12}(\omega)$; the first factor in brackets on the right-hand side as the transfer function of region 2, $H_2(\omega)$; and the second factor in brackets on the right-hand side as the power spectrum of the region 1 output, $\Phi_{11}(\omega)$. Equation (28) may now be written with equation (25) to give the relation of the cross-power spectrum between the outputs of region 1 and region 2 to their transfer functions, their power spectra, and the cross-power spectrum between the external input and the output of region 2.

$$\Phi_{12}(\omega) = A_1 e^{-j\omega\theta} H_2(\omega)\Phi_{11}(\omega). \qquad (29)$$

If there is no external input, equations (25) and (29) become,

$$\Phi_{12}(\omega) = A_2 e^{j\omega\theta} Y_1^*(\omega)\Phi_{22}(\omega) \quad \text{and} \qquad (30)$$

$$\Phi_{12}(\omega) = A_1 e^{-j\omega\theta} Y_2(\omega)\Phi_{11}(\omega) . \qquad (31)$$

It is noted that different symbols are used for the transfer functions in the set of equations (25) and (29) than in the set of equations (30) and (31). The reasons for so symbolizing these transfer functions are given in the next section.

Relations may also be established for the cross-power spectra between the external input and the outputs of the two regions. The relations are derived in the same manner as were those for $\Phi_{12}(\omega)$, and are,

$$\Phi_{i1}(\omega) = H_1(\omega)\Phi_{ii}(\omega) + A_2 e^{-j\omega\theta} H_1(\omega)\Phi_{i2}(\omega) \qquad (32)$$

and

$$\Phi_{i2}(\omega) = A_1 e^{-j\omega\theta} H_2(\omega)\Phi_{i1}(\omega). \qquad (33)$$

Two Region Transfer Functions

The two transfer functions, $H_1(\omega)$, and $H_2(\omega)$, are now derived from the reactor kinetics equations for a coupled reactor system. Each region is regarded as a subcritical reactor with a neutron leakage interaction from the other slab. Within each region the theory is space independent and a one group bare reactor model is assumed. Cohn (11) has commented that the one group bare reactor model is still used for practically all kinetics work, even though it has been discarded as impossibly crude for most statics calculations. His work shows that for most reflected reactors, the kinetic behavior corresponds to that of a bare reactor with the same l/v lifetime.

The kinetics equations for region 1 may then be written (18)

$$\frac{dn_1}{dt} = \frac{\left[k_1(1-\beta)-1 \right] n_1}{\ell} + \sum_i \lambda_i c_{i1} + S_1 + E \quad (34)$$

and

$$\frac{dc_{i1}}{dt} = \frac{\beta_i k_1 n_1}{\ell} - \lambda_i c_{i1} \quad . \qquad (35)$$

where, n_1 is the neutron density in region 1

k_1 is the effective multiplication factor for region 1

ℓ is the overall prompt neutron lifetime in the system

β_i is the fraction of fission neutrons in the i-th group of delayed neutrons and

$$\beta = \sum_i \beta_i$$

λ_i is the decay constant of precursor of i-th group of delayed neutrons

c_{i1} is the concentration of precursors of i-th group of delayed neutrons in region 1

S_1 is the neutron density from external source neutrons in region 1.

The term E is the interaction term caused by the leakage of neutrons out from region 2. This term may be represented by some fraction, A_2, of the neutron density in region 2 at some previous time corresponding to the transit time, θ, between regions. Thus

$$E = \frac{A_2 n_2(t - \theta)}{\ell} . \qquad (36)$$

Expanding this expression in a Taylor's series about t,

$$E = \frac{A_2 n_2(t)}{\ell} - \frac{A_2 \theta}{\ell} \frac{dn_2(t)}{dt} + \frac{A_2 \theta^2}{2 \ell} \frac{d^2 n_2(t)}{dt^2} - \ldots . \qquad (37)$$

Baldwin (17) estimates θ by assuming it to be determined by the mean thermal neutron velocity. In the UFTR, which has a 30 centimeter region of graphite between the fuel regions, this assumption would indicate a value of approximately 2×10^{-4} seconds for θ. Such a small value would make θ relatively unimportant in kinetics except for very short periods and unimportant in the transfer function except at very high frequencies. A more realistic assumption is that a disturbance in the neutron density in one fuel slab travels across to the opposite region with the velocity of a neutron wave. The velocity of a neutron wave is frequency dependent but at frequencies from 1 to 100 radians per second is approximately constant at 1.4×10^4 centimeters per second in graphite (22). This gives a lag time, θ, in the UFTR of about 2×10^{-3} seconds, a value that makes it desirable to retain at least the first few terms of the expansion of equation (37).

The kinetics equations for region 1 are then,

$$\frac{dn_1}{dt} = \frac{\left[k_1(1-\beta)-1\right] n_1}{\ell} + \sum_i \lambda_i c_{i1} + s_1$$

$$+ \frac{A_2 n_2}{\ell} - \frac{A_2\theta}{\ell}\frac{dn}{dt} + \frac{A_2\theta^2}{2\ell}\frac{d^2 n_2}{dt^2} - \cdots \qquad (38)$$

and

$$\frac{dc_{i1}}{dt} = \frac{\beta_i k_1 n_1}{\ell} - \lambda_i c_{i1}. \qquad (39)$$

A similar set of equations exists for region 2. In the experiment, a random reactivity input was given to region 1 only, while k_2 remained constant. This fluctuation in the multiplication factor in region 1 will give rise to fluctuations in the neutron density and delayed neutron precursor concentrations in both regions. There may also be fluctuations in the external neutron source. It is convenient then to linearize these quantities as follows:

$$\begin{aligned} n_1 &= n_{10} + \delta n_1 & n_2 &= n_{20} + \delta n_2 \\ k_1 &= k_{10} + \delta k_1 & c_{12} &= c_{i20} + \delta c_{12} \qquad (40) \\ c_{12} &= c_{i10} + \delta c_{i1} & s_1 &= s_{10} + \delta s_1 \end{aligned}$$

When these definitions are substituted into the equations of region 1, (38) and (39),

$$\frac{d}{dt}(n_{10}+\delta n_1) = \frac{\left[(k_{10}+\delta k_1)(1-\beta)-1\right](n_{10}+\delta n_1)}{\ell}$$

$$+\sum_i \lambda_i(c_{i10}+\delta c_{i1}) + s_{10}+\delta s_1 \tag{41}$$

$$+\frac{\lambda_2}{\ell}\left[(n_{20}+\delta n_2)-\theta\frac{d}{dt}(n_{20}+\delta n_2)+\frac{\theta^2}{2}\frac{d^2}{dt^2}(n_{20}+\delta n_2)+\dots\right]$$

and

$$\frac{d}{dt}(c_{i10}+\delta c_{i1}) = \frac{\beta_i(k_{10}+\delta k_1)(n_{10}+\delta n_1)}{\ell} - \lambda_i(c_{i10}+\delta c_{i1}). \tag{42}$$

The sums of the steady state portions of these equations are equal to zero, and the equations are linearized by setting the product, $\delta k\delta n$, equal to zero since both quantities will be small. The equations for region 1 are then

$$\frac{d\delta n_1}{dt} = \frac{(1-\beta)n_{10}\delta k_1}{\ell} + \frac{\left[k_{10}(1-\beta)-1\right]\delta n_1}{\ell} + \sum_i\lambda_i\delta c_{i1}$$

$$+\delta s_1 + \frac{\lambda_2}{\ell}\left[\delta n_2 - \theta\frac{d\delta n_2}{dt} + \frac{\theta^2}{2}\frac{d^2\delta n_2}{dt^2} - \dots\right], \text{ and} \tag{43}$$

$$\frac{d\delta c_{i1}}{dt} = \frac{\beta_i n_{10}\delta k_1}{\ell} + \frac{\beta_i k_{10}\delta n_1}{\ell} - \lambda_i\delta c_{i1} \tag{44}$$

When the Laplace transform, using zero initial conditions, is taken of both sides of both equations,

$$s\Delta N_1 = \frac{(1-\beta)n_1\Delta K_1}{\ell} + \frac{\left[k_1(1-\beta)-1\right]\Delta N_1}{\ell} + \sum_i \lambda_i \Delta c_{i1}$$
$$+\Delta\delta_1 + \frac{k_2}{\ell}\left[\Delta N_2 - \theta s\Delta N_2 + \frac{\theta^2}{2}s^2\Delta N_2 - \dots\right] \qquad (45)$$

and

$$s\Delta c_{i1} = \frac{\beta_i n_1 \Delta K_1}{\ell} + \frac{\beta_i k_1 \Delta N_1}{\ell} - \lambda_i \Delta c_{i1}, \qquad (46)$$

where s is the Laplace transform variable, the capital letters denote the Laplace transform of the δ quantities (i.e., ΔN_1 is the Laplace transform of δn_1), and the small letters are now understood to represent steady state values. Equation (46) may be solved for Δc_{i1}. When this is done and Δc_{i1} substituted into equation (45) and terms collected,

$$\left[s - \frac{k_1(1-\beta)-1}{\ell} + \frac{k_1}{\ell}\sum_i \frac{\beta_i\lambda_i}{s+\lambda_i}\right]\Delta N_1 =$$
$$= \Delta\delta_1 + \frac{(1-\beta)n_1}{\ell}\Delta K_1 + \frac{k_2}{\ell}\left[1-\theta s + \frac{\theta^2 s^2}{2} - \dots\right]\Delta N_2 \qquad (47)$$

If there is no disturbance of the multiplication factor in region 1, then equation (47) becomes,

$$\left[s - \frac{k_1(1-\beta)-1}{\ell} + \frac{k_1}{\ell} \sum_i \frac{\beta_i \lambda_i}{s+\lambda_i} \right] \Delta n_1$$

$$= \frac{\lambda_2}{\ell} \left[1 - \theta s + \frac{\theta^2 s^2}{2} - \dots \right] \Delta n_2 + \Delta \mathcal{S}_1 \tag{48}$$

Since k_2 is assumed to remain constant, the kinetics equations for region 2, after manipulations similar to the above, reduce to,

$$\left[s - \frac{k_2(1-\beta)-1}{\ell} + \frac{k_2}{\ell} \sum_i \frac{\beta_i \lambda_i}{s+\lambda_i} \right] \Delta n_2$$

$$= \frac{\lambda_1}{\ell} \left[1 - \theta s + \frac{\theta^2 s^2}{2} - \dots \right] \Delta n_1 + \Delta \mathcal{S}_2 . \tag{49}$$

The transfer function is defined as the ratio of the system output to the system input when both are expressed in Laplace notation. The inputs and outputs used to derive the transfer functions must correspond to the physical situation. It is not uncommon to speak of two different transfer functions in connection with subcritical reactors; a source transfer function and a reactivity transfer function. In the former, the input is associated with fluctuations in the external neutron source, while in the latter, fluctuations in the multiplication factor or reactivity are considered the input. In the two slab reactor system, each slab is considered as a subcritical system so the same logic should apply. The transfer function when an external reactivity input is applied to a slab is a reactivity transfer function, while the transfer function when there is no external input is a source transfer function; the leakage of neutrons from the opposite slab is considered as an external neutron source.

This source transfer function is easily recognized in the case of an external random input to slab 1 while the reactivity of slab 2 is held constant. The fluctuations in the multiplication factor of slab 1 cause fluctuations in the neutron population in that slab. A certain fraction, A_1, of this fluctuating population leaks out of region 1 and may be considered an external neutron source for region 2. This fluctuating neutron source then causes the neutron population of region 2 to fluctuate. A source transfer function for region 2 may then be formed by the ratio of the output of slab 2 to the output of slab 1 when both are in Laplace notation

When there is no external reactivity input to region 1 fluctuations still exist in the neutron population of that slab. These are the so-called self-fluctuations or reactor noise. The statistical nature of the fission process gives rise to these fluctuations in reactor power levels even when the reactor is operated at steady state. It has been shown (7) that the power spectrum of reactor (single region) self-fluctuations is related to the transfer function, $H(\omega)$ through,

$$\Phi_{11}(\omega) = Q + Q' \left| H(\omega) \right|^2 , \qquad (50)$$

where Q and Q' are constants. The expression has two terms, the first being white noise of the detector and the second being related to the kinetics parameters. The transfer function used is the one based on reactivity, although the exact input to the system is not definable (16).

Both slabs will exhibit these self-fluctuations, but crosscorrelation should measure the effect of the self-fluctuations of one region on the neutron density in the other region. The transfer functions to describe this situation would be source transfer functions, the self-fluctuations in one side acting as the input to the other side.

When a random reactivity input is given to region 1, the desired transfer function of that region is given by

$$H_1(\omega) = \frac{\Delta N_1/n_1}{\Delta K_1} \quad , \qquad (51)$$

where $\Delta N_1/n_1$ is the normalized output, and ΔK_1 is the input. This ratio is obtained from equation (47) after ΔN_2 is eliminated by substitution from equation (49). With the assumption of no external neutron source, solving equation (48) for ΔN_2 gives,

$$\Delta N_2 = \frac{\frac{A_1}{\ell}\left[1 - \theta s + \frac{\theta^2 s^2}{2} - \ldots\right]\Delta N_1}{s - \frac{k_2(1-\beta)-1}{\ell} + \frac{k_2}{\ell}\sum_i \frac{\beta_i \lambda_i}{s + \lambda_i}} \; . \qquad (52)$$

Substitution of this expression for ΔN_2 into equation (47) gives, after some algebraic manipulations and setting $s = j\omega$ and $e^{-j\omega\theta} = 1 - j\omega\theta + \frac{\omega^2\theta^2}{2} - \ldots$

$H_1(\omega) =$

$$\frac{(1-\beta)/\ell}{j\omega - \frac{k_1(1-\beta)-1}{\ell} + \frac{k_1}{\ell}\sum_i \frac{\beta_i\lambda_i}{j\omega+\lambda_i} - \frac{\frac{A_1A_2}{\ell}e^{-2j\omega\theta}}{j\omega - \frac{k_2(1-\beta)-1}{\ell} + \frac{k2}{\ell}\sum_i \frac{\beta_i\lambda_i}{j\omega+\lambda_i}}} \qquad (53)$$

The desired transfer function for region 2 when a random variation of reactivity is inserted in region 1 is a source-based transfer function and is given by

$$H_2(\omega) = \frac{\Delta_{N_2}}{\Delta_{N_1 A_1} e^{-j\omega\theta}} , \qquad (54)$$

where Δ_{N_2} is the output of region 2 and $\Delta_{N_1 A_1} e^{-j\omega\theta}$ is its input. $H_2(\omega)$ may be found from equation (49) directly. Thus from equation (49),

$$H_2(\omega) = \frac{\frac{1}{\ell}}{j\omega - \frac{k_2(1-\beta)-1}{\ell} + \frac{k_2}{\ell} \sum_{i} \frac{\beta_i \lambda_i}{j\omega + \lambda_i}} . \qquad (55)$$

When there is no external reactivity input to the two slab system, both transfer functions are thought of as source transfer functions in which the leakage from one side is considered a source to the other side. The transfer functions must then be formed by

$$Y_1(\omega) = \frac{\Delta_{N_1}}{\Delta_{N_2 A_2} e^{-j\omega\theta}}$$

$$Y_2(\omega) = \frac{\Delta_{N_2}}{\Delta_{N_1 A_1} e^{-j\omega\theta}} . \qquad (56)$$

$Y_1(\omega)$ may be formed directly from equation (48)

$$Y_1(\omega) = \frac{1/\ell}{j\omega - \frac{k_1(1-\beta)-1}{\ell} + \frac{k_1}{\ell}\sum_i \frac{\beta_i\lambda_i}{j\omega+\lambda_i}} , \qquad (57)$$

while $Y_2(\omega)$ is formed directly from equation (49), as was $H_2(\omega)$.

$$Y_2(\omega) = \frac{1/\ell}{j\omega - \frac{k_2(1-\beta)-1}{\ell} + \frac{k_2}{\ell}\sum_i \frac{\beta_i\lambda_i}{j\omega+\lambda_i}} . \qquad (58)$$

Reduction of Equations

If only the higher frequencies ($\omega > 1$) are considered so that the effects of delayed neutrons need not be considered, and the parameter B is defined as

$$B_1 = \frac{1 - k_1(1 - \beta)}{\ell} . \qquad (59)$$

then the four transfer functions are reduced to the following:

$$B_1(\omega) = \frac{(1-\beta)/\ell}{B_1 + j\omega - \dfrac{[A_1A_2/\ell]\, e^{-2j\omega\theta}}{B_2 + j\omega}} , \qquad (60)$$

$$B_2(\omega) = Y_2(\omega) = \frac{1/\ell}{B_2 + j\omega} , \qquad (61)$$

and

$$Y_1(\omega) = \frac{1/\ell}{B_1 + j\omega} . \qquad (62)$$

These expressions are now used in equations (25), (29), (30), (31) (32), and (33). When an external reactivity input is given to region 1,

$$\Phi_{12}(\omega) = \frac{(1-\beta)/\ell\left[\Phi_{12}(\omega) + A_2 e^{j\omega\theta}\,\Phi_{22}(\omega)\right]}{B_1 - j\omega - \dfrac{[A_1A_2/\ell^2]\, e^{2j\omega\theta}}{B_2 - j\omega}} , \qquad (63)$$

$$\Phi_{12}(\omega) = \frac{[A_1/\ell]\, e^{-j\omega\theta}\,\Phi_{11}(\omega)}{B_2 + j\omega} , \qquad (64)$$

$$\Phi_{11}(\omega) = \frac{(1-\beta)/\ell\left[\Phi_{11}(\omega) + A_2 e^{-j\omega\theta}\,\Phi_{12}(\omega)\right]}{B_1 + j\omega - \dfrac{[A_1A_2/\ell^2]\, e^{-2j\omega\theta}}{B_2 + j\omega}} \qquad (65)$$

and

$$\Phi_{12}(\omega) = \frac{[A_1/\ell]\, e^{-j\omega\theta}\, \Phi_{11}(\omega)}{a_2 + j\omega} \qquad (66)$$

The transit time between the regions, θ , has been considered independant of direction. Further simplification is effected if the slabs are assumed identical except for their multiplication factors which may be different. This assumption results in the condition

$$A_1 = A_2 = A , \qquad (67)$$

and equation (64) becomes,

$$\Phi_{12}(\omega) = \frac{[A/\ell]\, e^{-j\omega\theta}\, \Phi_{11}(\omega)}{a_2 + j\omega} . \qquad (68)$$

The expression for $\Phi_{12}(\omega)$ when there is no external reactivity input to region 1 is identical to equation (68). The power spectrum, $\Phi_{11}(\omega)$ is a real quantity but the cross-power spectrum is a complex quantity which may be expressed in terms of its phase and amplitude components. If the complex quantity $R_{12}(\omega)$ is defined as

$$R_{12}(\omega) = \frac{\Phi_{12}(\omega)}{\Phi_{11}(\omega)} , \qquad (69)$$

then it may be expressed in terms of its amplitude, $/R_{12}/$, and its phase, $p(R_{12})$, parts, as

$$/R_{12}/ = \frac{\frac{A^2}{\ell}\sqrt{2B_2^{\,2} + 2\omega^2}}{B_2^{\,2} + \omega^2} \tag{70}$$

and,

$$p(R_{12}) = \tan^{-1}\left[\frac{-\omega\cos\theta\omega - B_2\sin\theta\omega}{B_2\cos\theta\omega - \omega\sin\theta\omega}\right] . \tag{71}$$

Equation (70) shows that the amplitude portion of R_{12} is independant of θ and that the shape of $/R_{12}/$ depends only on the value of the multiplication constant of the region not disturbed by the random reactivity input. The phase portion of $R_{12}(\omega)$, however, is strongly dependent on the value of θ, particularly as the product $\theta\omega$ becomes large. Figures 2 and 3 show plots of the amplitude and phase portions of $R_{12}(\omega)$ versus frequency as calculated from equations (70) and (71) for a reactor of the geometrical arrangement of the UFTR. The normalized amplitude plot (Figure 2) is made for several values of B: 100, 200, 500, and 1000. These values correspond to multiplication factors of 0.97, 0.94, 0.85 and 0.70, respectively, for a neutron lifetime of 3×10^{-4} seconds. As noted before this plot is independent of

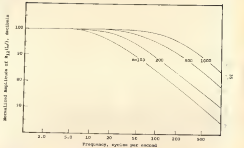

Figure 2. Normalized Amplitude Component of $R_{12}(\omega)$ for Several Values of B

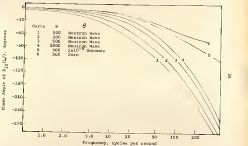

Figure 3 Phase Component of $R_{12}(\omega)$ for Several Values of B and θ

the transit time between slabs. The phase plot (Figure 3) indicates the dependance of the complex quantity $R_{12}(\omega)$ on this transit time, θ . For B=500, the phase plots for three different values of θ are shown: first, for θ equal to zero; second, for θ corresponding to the thermal neutron velocity; and third, for θ corresponding to the frequency dependent thermal neutron wave velocity. The value of the transit time between slabs in the UFTR when a disturbance on one side is assumed to travel to the other side with the velocity of a thermal neutron wave is calculated in Appendix A. The phase part of $R_{12}(\omega)$ is also given in Figure 3 for B values of 100, 200, and 1000, with θ corresponding to the thermal neutron wave velocity. It is seen that for a particular value of B, such as 500, the phase portion of the quantity $R_{12}(\omega)$ provides a rather sensitive test for the validity of assumptions about the nature of θ . The measurement of $R_{12}(\omega)$ would also allow the determination of the parameter, B, which yields information about the multiplication factor of the non-disturbed region. In a balanced reactor system such as the UFTR in which the multiplication factors of the two regions are equal, Baldwin (26)[17] has shown that

$$A = B\ell \quad . \tag{72}$$

Thus a determination of B yields information about the magnitude of the coupling of the two regions.

CHAPTER III

MEASURING SYSTEM

In this chapter are discussed methods and equipment used to perform the direct measurement of the cross-power spectrum of the outputs of the two regions of the UFTR. The first section contains a development of the relations necessary for the evaluation of the real and imaginary parts of the cross-power spectrum using band pass filters. These relations indicate the sequence of operations that must be executed. The second section contains a description of the University of Florida Training Reactor (UFTR). Since the measurements were made on this reactor, its pertinent features and dimensions are given. The third section examines in detail each component used to collect, store, and process data. The final section describes the random reactivity input device.

Measuring Theory

Most investigators have used autocorrelation and crosscorrelation measurements to obtain the transfer functions of single region reactor systems. This method lends itself well to digital processing of data. Results of auto or crosscorrelation measurements are in terms of the unit impulse response function, while the quantity of interest is the transfer function. The power and cross-power spectra, however, may be measured directly and, as seen from the previous chapter, relate directly to the system transfer functions.

The theory of the measurement of power and cross-power spectra is outlined below. The relation of the crosscorrelation function to the cross-power spectrum is,

$$\phi_{12}(\tau) = \int_{-\infty}^{\infty} \Phi_{12}(\omega)\, e^{j\omega\tau}\, d\omega . \qquad (17)$$

The definition of the crosscorrelation function,

$$\phi_{12}(\tau) = \lim_{T\to\infty} \frac{1}{2T}\int_{-T}^{T} f_1(t) f_2(t+\tau)\,dt, \qquad (1)$$

may be substituted into (17) to give

$$\lim_{T\to\infty} \frac{1}{2T}\int_{-T}^{T} f_1(t) f_2(t+\tau)\,dt = \int_{-\infty}^{\infty} \Phi_{12}(\omega)\, e^{j\omega\tau}\, d\omega . \qquad (73)$$

Here, $f_1(t)$ and $f_2(t)$ are voltages representing the neutron density in each slab. The integration over t cannot, of course, be performed over infinite time or over negative times, so a finite average is used, resulting in the approximation,

$$\frac{1}{T}\int_0^T f_1(t) f_2(t+\tau)\,dt = \int_{-\infty}^{\infty} \Phi_{12}(\omega)\, e^{j\omega\tau}\, d\omega \,. \tag{74}$$

The first operation in the data processing is to pass both signals through identical band pass filters, both of which are centered at the same frequency, ω_1, with the same frequency band width $\Delta\omega_1$. Equation (74) then becomes,

$$\frac{1}{T}\int_0^T f_1(t)\Big]_{\omega_1} f_2(t+\tau)\Big]_{\omega_1} dt = \Phi_{12}(\omega_1)\, e^{j\omega_1\tau}\, \Delta\omega_1 \,. \tag{75}$$

The power spectrum measurement, when $f_1(t)=f_2(t)$, is considered first; then,

$$\frac{1}{T}\int_0^T f_1(t)\Big]_{\omega_1} f_1(t+\tau)\Big]_{\omega_1} dt = \Phi_{11}(\omega_1)\, e^{j\omega_1\tau}\, \Delta\omega_1 \,. \tag{76}$$

If τ is set equal to zero equation (76) is then written

$$\frac{1}{T}\int_0^T \left[f_1(t) \right]^2_{\omega_1} dt = \Phi_{11}(\omega_1)\Delta\omega_1 \qquad (77)$$

where the left-hand side is the mean square value of $\left. f_1(t) \right]_{\omega_1}$. This expression is solved for $\Phi_{11}(\omega_1)$,

$$\Phi_{11}(\omega_1) = \frac{\int_0^T \left[f_1(t) \right]^2_{\omega_1} dt}{T\Delta\omega_1} \qquad (78)$$

Figure 4 indicates the sequence of operations necessary to solve equation (78) experimentally.

The cross-power spectrum is a complex quantity and may be expressed in terms of its real parts, Re_{12}, and its imaginary parts, Im_{12}. Use is also made of Euler's relation,

$$e^{j\omega_1\tau} = \cos\omega_1\tau + j\sin\omega_1\tau \qquad (79)$$

to reduce equation (75) to

$$\frac{1}{T}\int_0^T \left. f_1(t) \right]_{\omega_1} \left. f_2(t+\tau) \right]_{\omega_1} dt =$$

$$\left[Re_{12}\cos\omega_1\tau - Im_{12}\sin\omega_1\tau + j(Im_{12}\cos\omega_1\tau + Re_{12}\sin\omega_1\tau) \right] \Delta\omega_1. \qquad (80)$$

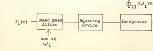

Figure 4. Sequence of Operations Necessary for Experimental Determination of Power Spectrum

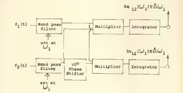

Figure 5. Sequence of Operations Necessary for Experimental Determination of Cross-Power Spectrum

When T is set equal to zero, equation (80) reduces to,

$$\frac{1}{T}\int_0^T f_1(t)\Big]_{\omega_1} f_2(t)\Big]_{\omega_1} dt = \Big[Re_{12} + jIm_{12}\Big]\Delta\omega_1. \tag{81}$$

The integral on the left side of this equation is a real quantity so that when the real parts are equated,

$$Re_{12}(\omega_1) = \frac{\int_0^T f_1(t)\Big]_{\omega_1} f_2(t)\Big]_{\omega_1} dt}{T\Delta\omega_1}. \tag{82}$$

Returning to equation (80) one sets T equal to $\frac{\pi}{2\omega_1}$. Since both $f_1(t)$ and $f_2(t)$ have been put through identical band pass filters and are both essentially at the same frequency, ω_1,

$$f_2\left\{t + \frac{\pi}{2\omega_1}\right\}\Big]_{\omega_1} = f_2(t + 90^\circ)\Big]_{\omega_1}. \tag{83}$$

Thus equation (80) becomes,

$$\frac{1}{T}\int_0^T f_1(t)\Big]_{\omega_1} f_2(t + 90^\circ)\Big]_{\omega_1} dt = \Big[-Im_{12} + jRe_{12}\Big]\Delta\omega_1. \tag{84}$$

Once again, the integral on the left side of equation (84) is recognized to be a real quantity, so that when the real parts are equated,

$$\mathrm{Im}_{12}(\omega_1) = \frac{-\int_0^T f_1(t)\Big]_{\omega_1} f_2(t + 90^\circ)\Big]_{\omega_1} dt}{T\Delta\omega_1} . \quad (85)$$

Equations (82) and (85) may be solved experimentally as shown in Figure 5.

The University of Florida Training Reactor

The UFTR is a 10kw heterogeneous, light water and graphite moderated, graphite reflected, thermal reactor of the Argonaut type (23). It may be fueled with either 20 or 93 per cent enriched uranium-aluminum fuel elements. The fuel is contained in thin flat plates which are assembled in bundles of eleven plates. The reactor core contains 24 bundles of fuel plates placed in six water-filled aluminum boxes surrounded by reactor grade graphite. Four cadmium control blades, protected by magnesium shrouds, move between the fuel boxes. Twelve inches of graphite separate the two rows of fuel boxes. Aluminum headers connect to the bottom of the fuel boxes and supply the light water used for moderating and cooling. The tops of the boxes are connected by aluminum overflow and vent pipes. This water, overflowing from the fuel boxes, flows by gravity through a cooling coil and then into a storage tank. The water is pumped from the storage tank to the fuel boxes. The storage tank prevents any sudden temperature changes in the coolant, its capacity being about six times that of the reactor system.

Air spaces 9 inches wide exist between the graphite reflector and the inside of the biological shield on the north and south sides of the reactor. The ion chambers used to detect the output of each region of the reactor were positioned in these spaces against the graphite, as shown in Figure 6. A graphite layer of 18 inches separated the chambers from the fuel boxes.

The UFTR is provided with six horizontal beam ports. These ports have a 4 inch diameter next to the core and increase to a 6 inch diameter through the rest of the shield. The core graphite stacking adjacent to the south beam port is fitted with a removable graphite plug 18 inches long by 2 inches diameter. When this plug is removed, the south beam port extends to the side of the south fuel box, at about the horizontal center plane of the core. The random reactivity device was inserted into the reactor through this facility.

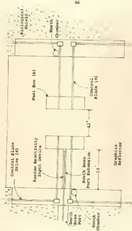

Figure 6. Location of Ion Chambers in UFTR Core

Cross-Power Spectrum Analyzer

The measurement of the cross-power spectrum between the outputs of the two regions of the UFTR involved both transcribing output signals on magnetic tape and subsequently processing these signals in the manner indicated in Figure 5. Figure 7 is a flow diagram of the equipment used to collect and store output signals of each region of the reactor on magnetic tape.

Fluctuations in the neutron intensity of each region were converted into current fluctuations by the two Westinghouse 6377 compensated ion chambers placed in the core. Two battery packs supplied 600 volts to each chamber. No compensating voltage was used. Each chamber was positioned outside one of the fuel slabs as shown in Figure 6. Attempts to avoid ground loops in the system included wrapping the ion chambers in transformer cloth and covering all connectors with electrical tape, since the chambers were in contact with the aluminum and graphite in the core. These precautions were found to eliminate from the measurements large amounts of 60 cycle interference.

About 15 feet of coaxial cable were used to connect the ion chambers with the Keithley Model 410 Micro-microammeters located immediately outside the UFTR

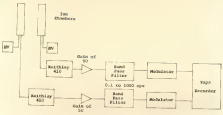

Figure 7. Data Transcribing System

shield. The micro-microammeters converted the signals from current fluctuations to voltage fluctuations which were then amplified on an Applied Dynamics Analog Computer located in the reactor control room, so that the ac portion of each signal was about 10 volts peak to peak. The analog computer was also used to buck-out the dc produced by the steady state power level of the reactor. Two Krohn-Hite Ultra-low frequency band pass filters were used as high and low pass filters. The low cut-off frequencies were set at 0.1 cycle per second to remove all dc and any slow drifts in reactor power. Frequencies above 1000 cycles per second were of no interest in this experiment and were removed by setting the high cut-off frequencies at 1000 cycles per second. The signals were then amplitude modulated on an 80,000 cycles per second carrier. Amplitude modulation recording and playback is subject to considerable fluctuation in over-all gain (24). Because only approximate spectra were required in order to determine the mechanism of the lag between regions and to test the feasibility of the measurement of the multiplication factors of the regions, AM recording was employed. AM recording and detection equipment was also available. A schematic of the modulator is shown in Figure 8.

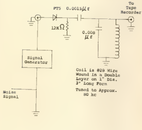

Figure 8. Modulator Schematic

The modulated signals were then recorded on two channels of an Ampex 500 magnetic tape recorder. A tape speed of 60 inches per second was used for both recording and playback. Modulation was necessary because of the frequency response of the tape recorder.

Figure 9 presents a flow diagram of the equipment used to measure the real and imaginary parts of the cross-power spectrum between the outputs of the two regions of the UFTR. The signals from the tape recorder were first demodulated, using the circuit shown in Figure 10. The demodulated signals were then amplified by a factor of about 25 on the analog computer in order to have signals of about 10 volts peak to peak to the band pass filters. The band pass filters were set for the same frequency and band width. A "zero" band width was used in which the upper and lower cut-off frequencies were set at the same value. The band pass filters allow frequencies outside the band width to pass through even though these "outside" frequencies are uniformly and greatly attenuated. When the upper and lower cut-off frequencies are equal to f_1, the half-power, or three db down, points are at $0.77f_1$ and $1.30f_1$. Thus, if a constant percentage or a "zero" band width is used, any error due to the "outside" frequencies is normalized. The larger the percentage band width used, the less the

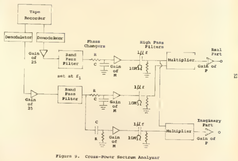

Figure 9. Cross-Power Sectrum Analyzer

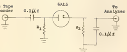

Demod #1	R_1 6.8KΩ	R_2 8.2KΩ
Demod #2	R_1 5.6KΩ	R_2 10KΩ

Figure 10. Demodulator Schematic

insertion losses in the filters become; however, the resolution also becomes poorer.

The two signals $f_1(t)\Big]_{\omega_1}$ and $f_2(t)\Big]_{\omega_1}$, were then given a phase lag in a low pass filter and $f_2(t)\Big]_{\omega_1}$ was also given a phase lead in a high pass filter such that there was a +90 degree shift between it and the lagging $f_1(t)\Big]_{\omega_1}$ and $f_2(t)\Big]_{\omega_1}$. The phase shifting networks were more complex than the simple filters indicated in Figure 9 because each filter fed into either a one megohm or a one-tenth megohm input resistor of an operational amplifier on the analog computer. Since the amplifier summing junctions are essentially at ground potential, either a one megohm or a one-tenth megohm resistor was in parallel with the capacitor, C, in the low pass filters and in parallel with the resistor, R, in the high pass filter. It is easily shown (25) that the amplitude, $|A|$, and the phase, p, portions of the transfer functions for these filters are given by, for the low pass filters,

$$|A|_L = \frac{K}{\sqrt{(R + K)^2 + R^2K^2\omega^2C^2}} \qquad (86)$$

and

$$P_L = \tan^{-1}\left[-\frac{RK\omega C}{R + K}\right] \qquad (87)$$

and for the high pass filter,

$$|A|_H = \frac{RK\omega C}{\sqrt{(R + K)^2 + R^2K^2\omega^2C^2}} \qquad (88)$$

and

$$P_H = \tan^{-1}\left[\frac{R + K}{RK\omega C}\right], \qquad (89)$$

where K is the value of the input resistor to the operational amplifier. Since the signals were passed through the band pass filters and were at essentially a single frequency, a convenient R and C were selected to give the desired 90 degree phase shift at each frequency set point. It was also found to be convenient to select a RC combination such that the amplitude, $|A|$, of the high pass and the low pass filters were equal at a given frequency. This was accomplished when

$$K = \frac{1}{\omega C} = \frac{1}{2\pi fC} \quad . \qquad (90)$$

Precision $\pm$0.1% polystyrene capacitors were available in values of 0.01, 0.1, and 1.0 microfarads and were used with precision $\pm$1% resistors and ten turn $\pm$3% 100KΩ potentiometers to set the C and R values of the filters. The capacitor and resistor values used are given in Appendix B.

It is noted that when an R and C are selected such that equation (90) is satisfied, the values of p_L and p_H are such that there is a +90 degree shift between them and the attenuation is the same through both filters. This attenuation is, however, frequency dependent. The calculation of correction factors for this attenuation is straightforward and also given in Appendix E.

The three signals, $\left.f_1(t)\right]_{\omega_1}$, $\left.f_2(t)\right]_{\omega_1}$ and $\left.f_2(t+90^\circ)\right]^{*}_{\omega_1}$ were then amplified by a factor of from about 20 to about 400 on the analog computer. This amplification was necessary in order to have signals of about 200 volts peak to peak for inputs into the Model 160 electronic multipliers on the analog computer. Large input signals are necessary to minimize the error that these diode network multipliers introduce for low input voltage.

---

*These symbols are now taken to represent the signals after they have passed through the phase shifting networks.

Before multiplication, however, the signals were passed through high pass filters to remove any dc components and low frequency drifts introduced because of the high gain of the system. The nominal 1.0 microfarad capacitors and 10 megohm resistors used were actually 1.09 microfarad and 9.9 megohms, but were matched to within 1 per cent. The outputs of these filters were fed into the one megohm input resistors of operational amplifiers. Here again, attenuation and phase shift were introduced, especially at the lower frequencies. The phase shift was identical for all three signals and was ignored. The amplitude attenuation is calculated in Appendix B.

Since both the phase changer and high pass filter attenuations were the same for $f_1(t)\Big]_{\omega_1}$, $f_2(t)\Big]_{\omega_1}$, and $f_2(t+90^\circ)\Big]_{\omega_1}$, the same correction was valid for all three. These corrections were squared, however, because the attenuations occurred before the multiplications. The separate and combined correction factors that were applied to the real and imaginary parts of the cross-power spectrum are given in Appendix B.

Multiplication was performed after the signals were passed through the high pass filters and the products $f_1(t)\Big]_{\omega_1} f_2(t)\Big]_{\omega_1}$ and $f_1(t)\Big]_{\omega_1} f_2(t+90^\circ)\Big]_{\omega_1}$ obtained. These products were then integrated and the integrals related to the real and imaginary parts of the cross-power spectrum. If the gain of the operational amplifiers between the band pass filters and the multipliers was M the gain of the integrators (1/RC) was P, the voltages on the integrators were V_R for the real and V_I for the imaginary parts for an integration time of T seconds and the set frequency and frequency band width were f_1 and Δf_1, respectively, then the real and imaginary parts of $\Phi_{12}(\omega)$ were given by,

$$Re_{12}(f_1) = \frac{V_R(CF)}{T\,\Delta f_1 (M)^2 P} \quad , \qquad (91)$$

and

$$Im_{12}(f_1) = \frac{V_I(CF)}{T\,\Delta f_1 (M)^2 P} \quad , \qquad (92)$$

where CF was the total correction factor for the amplitude attenuation of the phase shifters and high pass filters.

The measurement of the quantity $R_{12}(\omega)$ as defined by equation (69) requires that both the cross-power spectrum between both outputs and the power spectrum of the output of the externally excited region be measured. The real and imaginary parts of the cross-power spectrum were measured by use of equations (91) and (92). The power spectrum of region 1 was measured with the same computer setup as was the cross-power spectrum except that $f_1(t)$ only was used instead of $f_1(t)$ and $f_2(t)$. Since the power spectrum was a real quantity, there was only a voltage, V, on the integrator giving the real parts. For the same computer set-up as the cross-power spectrum, the power spectrum was given by,

$$\Phi_{11}(f_1) = \frac{V(CF)}{T \, \Delta f_1 (M)^2 P} \; . \tag{93}$$

Thus the real and imaginary parts of $R_{12}(f_1)$ were given by,

$$\mathrm{Re}\left[R_{12}(f_1)\right] = \frac{V_R}{V} \; , \tag{94}$$

and

$$\mathrm{Im}\left[R_{12}(f_1)\right] = \frac{V_I}{V} \; . \tag{95}$$

Thus the amplitude correction factors for the low and high pass filters were unnecessary in the calculation of $R_{12}(f)$. They were employed, however, when either the cross-power or the power spectra were measured.

Random Reactivity Input Device

The reactivity input system consisted of (a) a drive assembly of a coil in an electromagnet with spring return (b) an absorber in the form of a piston moving in a cylinder, (c) a power amplifier for the moving coil, and (d) a random input signal.

The drive and piston assembly was constructed by V. Rajagopal and is described in his doctoral dissertation (16). Figure 11 illustrates this assembly The drive assembly was a coil moving in the air gap of an electromagnet. The flux in the air gap was maintained by a steady current in the field coil. A 28 volt 3 amp power supply was used for the electromagnet. The force exerted by the moving coil was controlled by the current supplied from the power transistor in the power amplifier. Mechanical coupling from the moving coil to the cadmium covered piston was through a steel wire encased in a square slot between two blocks of graphite. The opposite end of the piston was connected

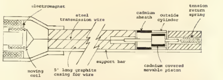

Figure 11. Random Reactivity Input Device

to a tension spring mounted inside a graphite block The graphite blocks and the cylinder of the absorber element were rigidly connected to the electromagnet.

A schematic diagram of the amplifier that drove the moving coil is given in Figure 12. The oscillator system was found to follow sinusoidal inputs in the frequency range 0.1 to 50 cycles per second at the maximum length of stroke (about 3/8 inch) while for higher frequencies, up to 100 cycles per second, about half stroke could be obtained. When the device was mounted in the south beam port, full stroke held about 0.015 per cent reactivity.

Two types of random noise generators were used as inputs to the power amplifier. The first was a commercial noise generator. The Elgenco, Inc., Low Frequency Noise Generator gave a 12 volt rms noise signal whose power spectrum was uniform from 0 to 35 cycles per second. The dc level of this signal was less than 50 millivolts.

A second random signal was constructed with a radioactive sample, GM counter, and a count rate meter. The signal was taken from the output of the flip-flop section of the count rate meter. This output was a randomly switched square wave whose mean period varied as the reciprocal of the count rate. This signal is

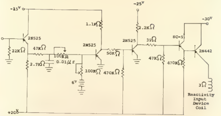

Figure 12. Power Amplifier Schematic

also called a "random telegraph signal" and its power spectrum is well known as (20)

$$\Phi_{ii}(\omega) = \left[\frac{4a^2g}{\pi}\right]\left[\frac{1}{\omega^2 + 4g^2}\right] , \qquad (96)$$

where g is the average number of sign changes per second of a square wave that varies between +a and -a. The power spectrum of this signal was then made white out to the desired frequency by a corresponding increase in the count rate seen by the GM tube. The signal was given the proper amplitude and dc level on the analog computer.

The reactivity device was sufficiently long to permit the piston end to be fully inserted into the south beam port extension, with the drive assembly outside the south reactor shield.

CHAPTER IV

EXPERIMENTS AND RESULTS

This chapter contains a description of the experiments performed both for check-out and calibration and for the measurement of the parameters of interest of the UFTR. This description includes data that were taken, data reduction, and the confidence limits assigned to the results. A detailed description of the procedure used to process the data is given in Appendix C.

The first section deals with the calibration runs in which the transfer function of a low pass filter was measured by obtaining the cross-power spectrum between a random input and the output of the filter from this input. The error analysis associated with this calibration is used with the data obtained from the reactor.

The second section presents data obtained from the reactor and data reduction. Data obtained both with and without an external input are presented.

Calibration

Performance of the cross-power spectrum analyzer and the data transcribing system were checked with the measurement of the transfer function of a low pass filter.

When a linear system is excited by a random input, the cross-power spectrum between the input and the output, $\Phi_{io}(\omega)$, is equal to the product of the power spectrum of the input, $\Phi_{ii}(\omega)$, and the transfer function of the system, $G(\omega)$ (19). The real and imaginary parts of the transfer function may be measured by,

$$\mathrm{Re}\left[G(\omega)\right] = \frac{\mathrm{Re}\left[\Phi_{io}(\omega)\right]}{\Phi_{ii}(\omega)}, \qquad (97)$$

and

$$\mathrm{Im}\left[G(\omega)\right] = \frac{\mathrm{Im}\left[\Phi_{io}(\omega)\right]}{\Phi_{ii}(\omega)}. \qquad (98)$$

The low pass filter the transfer function of which was measured, was formed by a one megohm resistor followed by a 0.1 microfarad capacitor to ground. These were precision ±1% components. The output of the filter fed a 0.1 megohm input resistor of an operational amplifier on the analog computer. The amplitude and phase parts of the transfer function, $G(\omega)$, were calculated from,

$$|A|_{G(\omega)} = \frac{K}{\sqrt{(R + K)^2 + R^2K^2\omega^2C^2}} \qquad (86)$$

and

$$P_{G(\omega)} = \tan^{-1}\left[-\frac{RK\omega C}{R + K}\right] , \qquad (87)$$

where

$K = 0.1\ M\Omega$
$R = 1.0\ M\Omega$
$C = 0.1\ \mu f.$

These two functions are plotted as solid lines versus frequency in Figures 13 and 14.

Performance of the cross-power spectrum analyzer independent of the data storage system was first examined by taking the cross-power and power spectra measurements "on line." A randomly switched step function was given as an input to the filter system. The step function was obtained from the flip-flop section of a count rate meter the input of which was supplied by a GM counter setup. The power spectrum of the input was measured as indicated by equation (93) and the real and imaginary parts of the cross-power spectrum as indicated by equations (91) and (92).

Two such runs were made, Run L and Run M. The only difference between these was that the GM counter set-up was adjusted to give a count rate of 1700 counts per minute in Run L and 13,500 counts per minute in Run M. Results of these runs are given in Tables 1 and 2 and plotted in Figures 13 and 14. The power spectrum of the random step input of Run L is also obtained from the measurement and given in Table 1. Note that the amplitude correction factors (Appendix B) must be used for the power spectrum. This measured spectrum is seen in Figure 15 with the theoretical spectrum as calculated for a q of 28.3 counts per second from equation (96).

The "flags" on the data points plotted in the above figures indicate one standard deviation. No "flags" are shown to indicate the accuracy of the frequency readings, which were determined by the accuracy of the settings on the band pass filters. The manufacturer gives ±5% as the accuracy of the frequency settings on the Krohn-Hite ultra low frequency band pass filters. It was necessary to calibrate the band pass filters against a frequency standard to match the filters to within one per cent of each other and the standard.

The non-statistical errors associated with the cross-power spectrum analyzer were small and are

TABLE 1

RESULTS OF RUN L

f cycles per second	Normalized Amplitude of $G(\omega)$ decibels	Phase Angle of $G(\omega)$ degrees	Normalized Power Spectrum of Input decibels
0.15	99.2	-0.6	99.1
0.2	97.6	-0.4	100.1
0.3	98.4	-4.6	99.0
0.4	99.0	-2.2	93.9
0.5	99.4	-1.1	98.3
0.6	101.4	-3.0	98.2
0.8	101.1	-4.2	97.9
1.0	100.0	-4.0	99.8
1.5	100.6	-6.7	98.7
2.0	100.6	-9.1	100.1
3.0	99.6	-12.4	98.4
4.0	99.4	-15.5	99.2
5.0	100.6	-18.0	97.7
6.0	100.0	-20.4	97.3
8.0	100.0	-26.1	94.6
10.0	99.4	-30.2	92.7
15.0	97.2	-39.0	88.3
20.0	96.2	-48.1	83.5
30.0	94.2	-57.3	77.3
40.0	93.6	-65.0	74.6
50.0	91.0	-66	70.3
60.0	90.2	-74	65.9
80.0	88.6	-79	61.5
100.0	88.2	-85	56.7
150.0	87.6	-86	48.4

TABLE 2

RESULTS OF RUN M

f cycles per second	Normalized Amplitude of G(ω) decibels	Phase Angle of G(ω) degrees
1.0	101.8	-5.3
1.5	100.2	-5.6
2.0	100.6	-9.9
3.0	100.6	-14.0
4.0	99.2	-15
5.0	100.1	-19
6.0	99.8	-18
8.0	99.6	-27
10.0	99.4	-32
15.0	98.4	-42
20.0	97.6	-54
30.0	94.6	-63
40.0	92.4	-68
50.0	92.0	-71
60.0	89.2	-75
80.0	87.2	-78
100.0	85.8	-82
150.0	85.4	-85

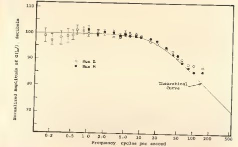

Figure 13. Normalized Amplitude Component of G(ω) from Runs L and M

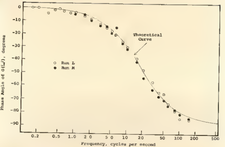

Figure 14. Phase Component of $G(\omega)$ from Runs L and M

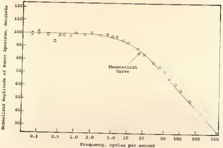

Figure 15. Normalized Power Spectrum of Random Step from Run L

estimated to be within 2 per cent. These errors are those associated with the components of the phase shifting network, potentiometer settings, computer amplifiers, multipliers, and the integrator amplifier readout. To hold these errors to within a few per cent, all potentiometer setting and amplifier readout was executed with the null potentiometer, all equipment allowed to warm up for an hour before data processing, and the amplifiers on the computer were balanced at frequent intervals.

The accuracy of the cross-power spectrum analyzer was limited primarily by statistical considerations. In the development of the theory of the measurement of power and cross-power spectra, it was necessary to form equation (74) from equation (73) by replacing an average over all time with a finite average time, T. The standard deviation expected from the effect of the finite averaging time has been derived by Bennett and Fulton (26). They give for the fractional standard deviation (σ/M) of a measurement of the power spectrum of normally distributed noise,

$$\sigma/M = \frac{1}{\sqrt{T\pi\Delta f}} \quad , \qquad (99)$$

where T is the integration time and Δf is the frequency difference between half-power points in the band pass filter. The expression may be used as a first order approximation to cases involving other distributions and spectral shapes as well as to cross-power spectra.

Three voltages were measured, V_R, V_I, and V, corresponding to the real and imaginary parts of the cross-power spectrum between the outputs of the two regions of the UFTR and to the power spectrum of the output of the externally disturbed region. Since the same integration times and frequency band widths were used for the measurement of all three voltages, all three have the same fractional standard deviation, namely,

$$\frac{\sigma}{V} = \frac{\sigma_R}{V_R} = \frac{\sigma_I}{V_I} = \frac{1}{\sqrt{\pi \tau \Delta f}} . \qquad (100)$$

In most cases, a three minute integration time was used. This value was taken as a compromise between the drift in the analog computer and a reasonable statistical accuracy.

Given the standard deviation of the voltage readings, the standard deviation of the amplitude and phase parts can be calculated from the propagation of errors formula

$$\sigma_f = \sqrt{\left[\frac{\partial f}{\partial x}\right]^2 \sigma_x{}^2 + \left[\frac{\partial f}{\partial y}\right]^2 \sigma_y{}^2} \quad , \qquad (101)$$

which gives the standard deviation, σ_f, of a function f(x,y) of the two quantities x and y which have standard deviations, σ_x and σ_y, respectively.

The above expression gives the standard deviation of the phase part (given by the quotient V_I/V_R) as,

$$\sigma_p = \frac{V_I}{V_R}\sqrt{\frac{2}{\pi \tau \Delta f}} \quad , \qquad (102)$$

and the standard deviation of the amplitude part (given by $\sqrt{\left[\frac{V_R}{V}\right]^2 + \left[\frac{V_I}{V}\right]^2}$) as,

$$\sigma_{|A|} = \sqrt{\frac{\left[\frac{V_R}{V}\right]^4 + \left[\frac{V_I}{V}\right]^4}{\left[\frac{V_R}{V}\right]^2 + \left[\frac{V_I}{V}\right]^2} \quad \frac{8}{\pi \tau \Delta f}} \qquad (103)$$

As seen in Figure 13, the standard deviation of the amplitude part at the lower frequencies is rather large. The standard deviation of the phase part, however, is of a magnitude comparable with the size of the data points.

The data of these figures do, however, indicate the satisfactory performance of the cross-power spectrum analyzer. The data of Figure 15 demonstrate that with the correction factors of Appendix B the analyzer may also be used successfully for the measurement of power spectra.

Referring to Figure 13, one observes that the data of Run L depart from the theoretical amplitude at frequencies beyond 50 cycles per second. This departure is a leveling out of the amplitude plot to the noise level of the analyzer. At 50 cycles per second Figure 15 shows that the random input power spectrum is down more than 30 decibels from the value at the lower frequencies. In Run M the power spectrum of the input carries more of the high frequency components and because of this, the cross-power spectrum data extend out to about 100 cycles per second. The phase data points followed the theoretical curve out to 125 cycles per second for both runs.

Run P was a run of the same type as L and M, but instead of processing the data "on line," the two signals, the random step input and the filter output, were AM modulated and stored on magnetic tape. The random step was formed from a count rate of 7100 counts per minute from the GM counter. The data from Run P as processed from the tape are given in Table 3. The data points of the amplitude and phase parts of the transfer function of the filter, $G(\omega)$, are shown plotted versus frequency in Figures 16 and 17. Once again, the theoretical curves are given also. The data from this run seem more scattered than the data points of Runs L and M, especially those of the amplitude part. This additional scatter must be attributed to the AM modulation, recording, and demodulation. The magnitude of the amplitude scatter is about ± 2 decibels while little difference is noted in the phase part. In all other respects the results of Run P were identical to those of Runs L and M. The amplitude portion of the data departs from the theoretical curve between 60 and 100 cycles per second, a higher frequency than that at which the departure occurred in Run L and a lower frequency than that at which the departure occurred in Run M. This was to be expected since the random input was driven by a count rate higher than Run L and lower than Run M.

Run P demonstrates that the techniques and equipment used to collect, record, and analyze the data were satisfactory.

TABLE 3

RESULTS OF RUN P

f cycles per second	Normalized Amplitude of $G(\omega)$ decibels	Phase Angle of $G(\omega)$ degrees
0.6	95.8	-6.1
0.8	101.2	-1.2
1.0	99.0	-6.7
1.5	98.4	-4.1
2.0	96.6	-6.5
3.0	98.6	-10
4.0	100.8	-18
5.0	98.2	-18
6.0	99.4	-25
8.0	97.0	-33
10.0	98.4	-30
15.0	100.0	-37
20.0	96.8	-51
30.0	94.2	-60
40.0	93.6	-62
50.0	90.8	-70
60.0	89.8	-72
80.0	89.2	-77
100.0	86.4	-80
150.0	86.6	-90

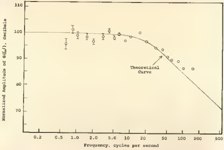

Figure 16. Normalized Amplitude Component of G(ω) from Run F

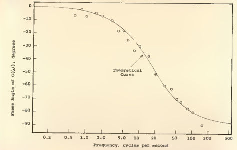

Figure 17. Phase Component of G(ω) from Run P

Reactor Data

Some of the first reactor data were taken "on line." The external reactivity input device used for these runs was driven by a random step function at an average count rate of 200 counts per minute. Because of the low count rate and inadequate frequency response of the reactivity input, the data obtained were not reliable at frequencies beyond about two cycles per second. Although the data looked promising out to this point, little could be determined, as seen from Figures 2 and 3.

The random input device designed and constructed by Rajagopal and described in the previous chapter was used in succeeding runs. These runs were recorded and processed "off line."

The reactor was fueled with 3100 grams of uranium-235 in the form of 93 per cent enriched uranium-aluminum fuel plates for Run R. The commercial low frequency noise generator was used as an input to the driving amplifier of the input device and the data were recorded with the reactor operating at a power level of 10 watts. The two Keithley micro-microammeters were operated on the $3x10^{-6}$ ampere scale. The results of this run are given in Table 4. Not only the phase and amplitude parts of the function $R_{12}(\omega)$ but also the

TABLE 4

RESULTS OF RUN R

f cycles per second	Normalized Amplitude of $R_{12}(\omega)$ decibels	Phase Angle of $R_{12}(\omega)$ degrees	Normalized Power Spectrum of Output of Region 1 decibels
0.6	98.8	-6.2	78.9
0.8	100.5	0	88.3
1.0	99.7	-7.0	89.2
1.25	99.3	-5.0	99.6
1.5	101.7	-0.7	98.5
2.0	99.5	-14	101.6
2.5	102.7	-7.0	99.4
3.0	99.3	-11	101.3
4.0	98.3	-13	99.0
5.0	100.1	-12	98.1
6.0	99.3	-15	95.0
7.0	103.1	-17	91.6
8.0	99.9	-16	93.1
9.0	99.7	-23	89.8
10.0	98.9	-26	90.6
12.5	98.7	-20	85.0
15.0	101.3	-28	79.2
20.0	97.8	-39	76.4
25.0	96.5	-45	71.4
30.0	95.6	-40	70.2
40.0	91.5	-34	68.7
50.0	88.7	-19	70.4
60.0	89.3	-3.2	71.1
70.0	86.5	0	70.2
80.0	85.3	-13	66.9
100.0	79.1	-44	64.6

power spectrum of the output of the south region (the externally disturbed region) are given. The amplitude part of $R_{12}(\omega)$, the phase part of $R_{12}(\omega)$, and the power spectrum of the output of the south region are plotted versus frequency in Figures 18, 19, and 20, respectively.

The phase data points, up to about 25 cycles per second, although badly scattered, are seen to follow the set of theoretical curves calculated for a lag time between the two reactor regions corresponding to the velocity of a thermal neutron wave. A B value of about 400 is indicated. Beyond a frequency of 25 cycles per second, little can be determined because of the excessive scatter of the data. The amplitude data points depart from the theoretical curve for a B of 400 beyond 15 cycles per second. It is difficult to determine whether this break in the amplitude data actually reflects a low value of B or if it signifies the end of correlation between the two reactor output signals because of low signal to noise ratio. The phase data would suggest the latter condition. Consideration of the power spectrum of the output of the south fuel slab (Figure 20) would also indicate that correlation would end much beyond 20 cycles per second. This power spectrum, which is representative of the

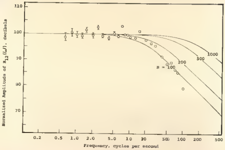

Figure 18. Normalized Amplitude Component of $R_{12}(\omega)$ from Run R

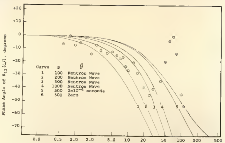

Figure 19 Phase Component of $R_{12}(\omega)$ from Run R

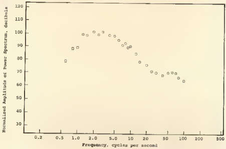

Figure 20. Normalized Power Spectrum of Region 1 Output from Run R

input to the north slab, ie down about 20 decibels at 15 cycles per second from the amplitude value at the lower frequencies. Except for a hump at 60 cycles, the power spectrum levels out to the reactor and instrument noise level at frequencies beyond 25 cycles per second. Since the random reactivity input device had been found to respond satisfactorily to sinusoidal inputs from 0.1 to 25 cycles per second, the cause of the drop-off of the power spectrum at the lower frequencies was unknown.

Full stroke of the device held about 0.007 per cent reactivity. When the noise generator was used to drive the reactivity input device, its effect could not be seen by the reactor operators on the console instrumentation. Observation of the signal from either of the chambers in the reactor revealed that the input disturbance was about one-half the magnitude of the inherent reactor noise.

To obtain a larger input reactivity disturbance the absorber piston assembly was reconstructed so as to be about double the exposed cadmium area. The tension spring was changed and the power amplifier was also modified to obtain better frequency response. With these modifications, the device was found to respond faithfully to sinusoidal inputs up to 50 cycles per second. Full stroke was found to produce more than 0.015 per cent reactivity change in the reactor.

For Run CC the reactor was fueled with 3500 grams of uranium-235 in the form of 20 per cent enriched uranium-aluminum alloy fuel plates. The reactor was operated at a power level of 50 watts and the two Keithley micro-microammeters were operated on the 3×10^{-6} ampere scale. The random reactivity input device was found to produce disturbances of almost twice the magnitude of the normal reactor noise. The power amplifier was driven by a randomly switched square wave. This random square wave was constructed with a GM counter and the flip-flop section of a count rate meter. A count rate of 20,000 counts per minute was used.

The results of Run CC are presented in Table 5. Once again the phase part of $R_{12}(\omega)$, the amplitude part of $R_{12}(\omega)$, and the power spectrum of the output of the south fuel region are listed in Table 5 and also plotted versus frequency in Figures 21, 22, and 23, respectively.

The phase data points, up to a frequency of 40 cycles per second, follow the theoretical curve corresponding to a B of about 450 and a lag time, θ determined from the velocity of a thermal neutron wave. Beyond 40 cycles per second, the data points become excessively scattered. The amplitude data points break from the theoretical curve for a B of 450 at frequencies beyond 25 cycles per second. Again, it is difficult to

TABLE 5

RESULTS OF RUN CC

f cycles per second	Normalized Amplitude of $R_{12}(\omega)$ decibels	Phase Angle of $R_{12}(\omega)$ degrees	Normalized Power Spectrum of Output of Region 1 decibels
0.4	101.0	0	101.4
0.5	99.5	-2.0	102.1
0.6	100.7	-5.3	100.7
0.8	100.0	0	99.3
1.0	102.0	-4.4	99.5
1.25	98.5	-2.0	102.6
1.5	101.1	-2.1	99.2
2.0	102.2	-5.1	98.8
2.5	99.2	-5.2	100.1
3.0	100.0	-7.0	97.0
4.0	102.0	-8.5	95.8
5.0	99.2	-10	94.7
6.0	101.4	-11	90.9
7.0	101.6	-14	89.7
8.0	99.0	-17	88.3
9.0	100.7	-18	85.7
10.0	98.7	-25	84.9
12.5	100.2	-22	78.0
15.0	100.2	-25	71.5
20.0	99.0	-39	66.3
25.0	100.0	-43	59.3
30.0	95.6	-49	58.0
40.0	93.9	-64	52.8
50.0	99.4	-65	52.3
60.0	90.5	-34	53.0
70.0	93.4	-62	48.7
80.0	83.7	-84	48.9
90.0	83.5	-56	48.6
100.0	80.9	-62	47.7
125.0	81.9	-70	46.3
150.0	80.4	-116	43.3

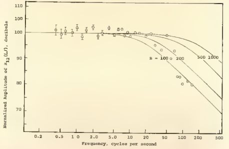

Figure 21 Normalized Amplitude Component of $R_{12}(\omega)$ from Run CC

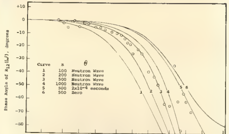

Figure 22. Phase Component of $R_{12}(\omega)$ from Run CC

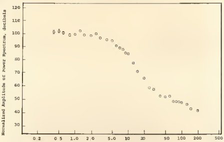

Figure 23. Normalized Power Spectrum of Region 1 Output from Run CC

determine if the break represents a lower value of B or if it represents the end of correlation. The power spectrum of the region 1 output indicates that correlation would end much beyond 25 or 30 cycles per second. At 30 cycles per second the power spectrum is down 40 decibels from the amplitude at the lower frequencies. From the calibration runs it would be expected that correlation would not continue when the input (which is the output of the south fuel region in this case) power spectrum drops off 40 decibels. There was no drop-off of the spectrum at the lower frequencies as in Run R, indicating a more satisfactory operation of the reactivity input device. The magnitude of the input signal was also greater than before resulting in the lower frequency portion of the spectrum being 50 decibels above the reactor and instrument noise level.

A check was made on the frequency at which correlation between the two outputs of the reactor ended with a complementary run to Run CC. Run 2 was taken under the same operational conditions as Run CC except that both ion chambers were located side by side outside the south fuel region. The results of this run are presented in Table 6. The amplitude and phase parts of the cross-power spectrum and the power spectrum of the output of the south fuel region are plotted versus frequency in Figures 24, 25, and 26, respectively.

TABLE 6

RESULTS OF RUN 2

f cycles per second	Normalized Amplitude of Calibration Spectrum decibels	Phase Angle of Calibration Spectrum degrees	Normalized Power Spectrum of Output of Region 1 decibels
0.4	99.9	+3.0	100.1
0.5	99.3	-0.8	103.1
0.6	101.7	-0.9	99.5
0.8	98.1	-1.5	101.3
1.0	101.0	+2.0	101.2
1.25	101.2	+0.5	99.3
1.5	98.6	-0.5	100.2
2.0	101.0	0	100.7
2.5	100.5	0	99.6
3.0	99.9	-0.6	97.9
4.0	101.7	0	97.4
5.0	101.0	0	93.8
6.0	97.2	-3.0	94.6
7.0	101.7	-1.3	89.9
8.0	100.1	-0.5	87.1
9.0	96.8	-0.7	87.7
10.0	101.4	-7.7	83.6
12.5	99.9	+3.6	77.9
15.0	97.8	-4.5	75.4
20.0	98.9	0	67.3
25.0	96.9	-2.0	63.0
30.0	94.4	-7.5	60.0
40.0	93.8	-10.0	55.6
50.0	87.0	-5.6	55.7
60.0	80.7	-11.0	56.0
70.0	84.6	+8.4	54.4
80.0	80.7	+13.0	53.0
90.0	79.6	-13.0	52.5
100.0	85.5	-44	50.5
125.0	80.2	-70	48.4
150.0	80.1	+98	47.4
200.0	79.9	-132	46.3

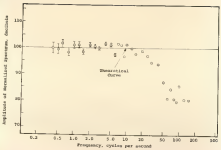

Figure 24 Amplitude Component of Normalized Cross-Power Spectrum from Run Z

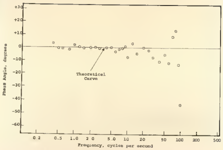

Figure 25 Phase Component of Normalized Cross-Power Spectrum from Run 2

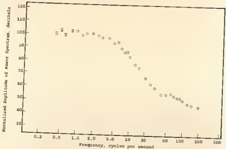

Figure 26. Normalized Power Spectrum of Region 1 Output from Run 2

The amplitude data points clearly indicate a loss of correlation beyond frequencies of 20 cycles per second. The cross-power spectrum between the ion chambers should be identical to the output power spectrum of the region if there is sufficient signal above the instrumentation and detection noise level. When the amplitude part of this cross-power spectrum is normalized by the output power spectrum of the region as determined by one of the chambers, a constant amplitude plot should result. This constant amplitude is the theoretical curve given in Figure 24. The drop-off beyond 20 cycles per second indicates that there is no correlation between the two ion chambers beyond this frequency. This end of correlation is also indicated by the phase part data points. There would be no phase shifting between the two chambers if perfect correlation existed. The zero phase angle line is plotted in Figure 25. Beyond 20 cycles per second, the data scatter indicates a loss of correlation. The output power spectrum of the south region as determined by one of the chambers is identical to that measured in Run CC.

When there was no external reactivity input to the reactor, no correlation could be detected between the outputs of the two fuel regions. The data for Run Q were collected while the reactor was fueled with the 93 per cent enriched fuel and operating at a power level of one watt. The Keithley micro-microammeters were operated on the 10×10^{-8} ampere scale. No external reactivity input was used. Table 7 gives the data, plotted in Figure 27, from Run Q of the power spectrum of the output of the south region of the reactor This spectrum is almost white. The detection chambers were located about 18 inches from the fuel slab in positions of low efficiency. It has been found (12) (16) that in such chambers the uncorrelated chamber noise dominates the signal, and the spectra found from them are almost flat.

TABLE 7

RESULTS OF RUN Q

f cycles per second	Normalized Power Spectrum of Output of Region 1 decibels
0.4	97.6
0.5	95.6
0.6	102.1
0.8	96.0
1.0	102.9
1.25	99.7
1.5	105.2
2.0	100.9
2.5	103.1
3.0	103.7
4.0	101.8
5.0	97.6
6.0	96.7
7.0	98.2
8.0	97.7
9.0	92.8
10.0	93.9
12.5	92.4
15.0	91.9
20.0	86.3
25.0	88.9
30.0	87.8
40.0	90.2
50.0	92.4
60.0	91.6
70.0	90.7
80.0	91.6
90.0	93.2
100.0	91.6
125.0	91.2
150.0	93.6
200.0	96.9

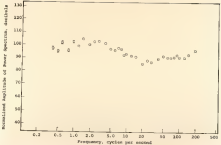

Figure 27. Normalized Power Spectrum of Region 1 Output from Run Q

CHAPTER V

DISCUSSION AND CONCLUSIONS

Of particular interest in this study was the representation of the coupling or interaction between the two fuel regions of a two slab reactor. The measurement of the complex quantity $R_{12}(\omega)$ in the University of Florida Training Reactor indicates that the relatively simple two point one group bare reactor model used in this thesis will give an adequate description of the kinetics of a two region reactor. The success of this representation does, however, depend on the value taken for the transit time of a disturbance between the two regions. The data that have been taken from the UFTR (in particular the phase part of Run CC, Figure 22) indicate that an adequate representation of the transit time, θ, is one in which a disturbance in the neutron density in one fuel slab travels to the opposite region with the velocity of a neutron wave.

These data have also indicated the feasibility of determining the multiplication factor of each of the regions by the measurement of the cross-power spectrum between the outputs. From the measurement of the quantity $B_{12}(\omega) = B$ (defined as $1 - k[1 - \beta]/\ell$) value of 450 is indicated for the multiplication factor of one region independent of the other. This value was taken from the phase data points only. It was not possible to obtain a value from the amplitude data points since the correlation between the two chambers ended at a frequency lower than the break frequency corresponding to a B value of 450. The phase data are sufficient, however, to establish a value of B. The calibration data indicated that the phase data points were reliable out to higher frequencies than were the amplitude data points.

This value of B is in good agreement with recent measurements by Badgley (27). Badgley measured subcritical multiplication constants for the UFTR for both one and two slab fuel loadings. Extrapolation of his results indicates a B value of 480±50 for a one slab loading of 1610 grams of uranium-235 in the 93 per cent enriched fuel plates. Chastain (28) gives an ℓ value of 2.8×10^{-4} seconds,* measured by a pile oscillator. For a neutron lifetime of 2.8×10^{-4} seconds, a α value of 450 corresponds to a multiplication factor of 0.874. Critical loading data with the 93 per cent enriched fuel indicate that the reactor would be critical with a one slab loading of 2005 grams of uranium-235. With a normal two slab loading of the fully enriched fuel, a total loading of 3225 grams of uranium-235, or 1612.5 grams per slab, produces a critical mass. The two regions are therefore very strongly coupled the interaction between them is worth about 390 grams of uranium-235. As much as 1950 grams of uranium-235 can be loaded into one region of the reactor. These attempts to load the reactor to critical in a one slab configuration gave not only an estimate of the critical mass but also an estimate of the multiplication factor for a given mass of fuel. For a uranium-235 mass of 1612.5 grams, the following estimates of the effective multiplication factor were obtained: loading of May 25, 1961, 0.87±0.08; loading of March 21, 1962, 0.79±0.08, loading of April 3, 1962, 0.82±0.08; and loading of June 15, 1962, 0.76±0.08. These results may be summarized to give a multiplication factor of 0.81±0.04 for one region independent of the other when the two slab system is critical. This value is in fair agreement with the α value of 450 obtained by the cross-power spectrum measurement.

---

*Chastain actually reports a prompt neutron lifetime of 2.4×10^{-4} seconds based on a delayed neutron fraction of 0.0065. In a compact core such as that of the UFTR an effective delayed neutron fraction of about 0.0075 should be used. His data then give a neutron lifetime of 2.8×10^{-4} seconds.

The UFTR is certainly not the ideal reactor on which to conduct a study of loosely coupled two region reactors since its two fuel regions are separated by only 12 inches of graphite and are rather strongly coupled. This strong coupling results in a large value of B which moves the break frequency of the amplitude part of $K_{12}(\omega)$ toward the higher frequencies. In order to measure this break frequency, the input to the second region should contain sufficient power in all frequencies out to and slightly beyond the break frequency. Although the random reactivity input device may deliver a signal whose power spectrum is flat beyond the break frequency of interest, the fuel slab that receives this signal acts very much as a low pass filter and will attenuate the higher frequencies. Thus the input to the second fuel slab will not necessarily have a flat power spectrum beyond the break frequency. It is felt that the UFTR is probably as strongly coupled a reactor for which the cross-power spectrum between the outputs of the two regions will give information.

Several equations were developed in Chapter II involving the cross-power spectra between the two outputs of the fuel regions and between the random reactivity input and each of the fuel region outputs.

Of these several equations, only one was developed for experimental use. In making measurements on a more complex reactor than the UFTR other of the equations may prove useful for experimental purposes.

This thesis was devoted to the treatment of a two region reactor system. The general method and experimental approach could certainly be extended to a three or more region system. Several large reactors have either been designed or built that have cores composed of several rather independent regions. An extension of the method developed in this thesis would allow the measurement of the multiplication factor of each region by crosscorrelating the outputs of two regions when a random disturbance is given to one region only.

The physical arrangement of the UFTR made it impossible to position the two ion chambers used to collect data any closer than 18 inches from each fuel region without extensive modifications of the graphite reflector surrounding the core. This fact meant that the detectors were located in positions of low efficiency (less than 10^{-4}). While this had no effect on the data taken when there was an external reactivity input to one region, it is felt that these low chamber efficiencies were responsible for the lack of correlation between the two region outputs where there was no external input

APPENDIX A

CALCULATION OF TRANSIT TIME BETWEEN SLABS

In this section a theoretical determination of the lag time, θ , of a neutron wave traveling between the two regions of the UFTR is made. It is assumed that the neutron wave originates in the center of one fuel slab and travels to the center of the opposite slab.

The velocity V, of a neutron wave corrected for leakage, is given by (22):

$$V(\omega) = \omega \left[\frac{2}{\left[\delta^4 + \left(\frac{\omega}{vD} \right)^2 \right]^{1/2} - \delta^2} \right]^{1/2} , \qquad (104)$$

where ω = frequency, radians per second

D = diffusion coefficient

$\delta^2 = (\pi/a)^2 + (\pi/b)^2 + (1/L)^2$

a,b = transverse dimensions of the wave

L = diffusion length

v = neutron velocity.

Thompson (29) gives the following values at thermal energies for the fuel and graphite regions of the UFTR:

	Fuel	Graphite
D	0.25 cm.	0.917 cm.
Σ_a	0.08112 cm.$^{-1}$	0.000342 cm.$^{-1}$
L	1.76 cm.	51.8 cm.

These results are given for a fuel slab consisting of a homogeneous mixture of water, aluminum, and uranium. It is also assumed that the reactor is loaded with 3500 grams of the 20 per cent enriched fuel.

For the reactor loaded with 3100 grams of the fully enriched fuel, Σ_a for the fuel section is 0.0723 centimeters^{-1}. The diffusion coefficient and diffusion length of the fuel region will also change from the values given for the 20 per cent enriched fuel. These changes are small enough, however, and the lag time in the fuel is a small enough fraction of the total lag time, that the values for the 20 per cent enriched fuel may be used for the fully enriched fuel also.

The dimensions a and b are taken as 264 and 142 centimeters. These dimensions correspond to the complete diffusion interface and include some of the graphite surrounding the fuel slab. The neutron velocity is taken as 2200 meters per second.

In the fuel section then

$$\delta^2 = \left[\frac{\pi}{264}\right]^2 + \left[\frac{\pi}{142}\right]^2 + \left[\frac{1}{1.76}\right]^2 \qquad (105)$$

$$\delta^2 = 0.3234.$$

Since the wave must travel through halves of two fuel sections, the lag time through one full fuel section is calculated. This lag time may be found by dividing the thickness of the fuel region, 13.34 centimeters, by the wave velocity as determined by equation (104). Substitution of the fuel region value gives,

$$\theta_{\text{fuel}} = \frac{4.02\text{x}10^{-2}}{\omega} \left[\left[(1.78\text{x}10^4)^2 + \omega^2\right]^{\frac{1}{2}} - 1.78\text{x}10^4 \right]^{\frac{1}{2}} . \qquad (106)$$

The expansion

$$(1 + x)^{\frac{1}{2}} = 1 + \frac{1}{2}x - \frac{1}{8}x^2 + \frac{1}{16}x^3 - \dots \qquad (107)$$

is useful in the evaluation of θ_{fuel} for small values of ω. The value of the lag time in the fuel at various frequencies is given in Table 8.

TABLE 8

VALUE OF TRANSIT TIME BETWEEN SLABS

Frequency cycles/second	Lag Time in Milliseconds		
	Fuel	Graphite	Total
0.5	0.213	2.39	2.60
1	0.213	2.39	2.60
2	0.213	2.39	2.60
5	0.213	2.39	2.60
10	0.213	2.35	2.56
20	0.213	2.26	2.47
50	0.213	1.99	2.20
100	0.213	1.63	1.84
200	0.213	1.25	1.46
500	0.213	0.830	1.04
1000	0.209	0.594	0.803

The value of δ^2 in the graphite region is found to be

$$\delta^2 = \left[\frac{\pi}{264}\right]^2 + \left[\frac{\pi}{142}\right]^2 + \left[\frac{1}{51.8}\right]^2$$

$$\delta^2 = 0.001012 \ . \tag{108}$$

The thickness of the graphite section separating the two fuel regions is 30.48 centimeters. When this distance is divided by the velocity of a neutron wave in graphite as determined by equation (104), the quotient is the lag time in the graphite.

$$\theta_{\text{graphite}} = \frac{4.80\text{x}10^{-2}}{\omega} \left[\left[(2.04\text{x}10^2)^2 + \omega^2 \right]^{\frac{1}{2}} - 2.04\text{x}10^2 \right]^{\frac{1}{2}} . \tag{109}$$

Values of the lag time in the graphite and the total lag time are also given in Table 8.

APPENDIX 5

PHASE SHIFT AND HIGH PASS FILTER DETAILS

In the measurement of the cross-power spectrum between two signals it was necessary to pass the signals through band pass filters, set around the same frequency, and then to introduce a 90 degree phase shift between them. This was accomplished by giving one signal a phase lag in a low pass filter and the other a phase lead in a high pass filter such that there was a 90 degree shift between them. The low pass filter was formed by a resistor, R, followed by a capacitor, C, and another resistor, K, in parallel to ground while the high pass filter was composed of a capacitor, C, followed by two resistors R and K, in parallel to ground. The amplitude, $/A/$, and phase, p, parts of the transfer functions for these filters are given by, for the low pass filter,

$$/A/_L = \frac{K}{\sqrt{(R + K)^2 + R^2K^2\omega^2C^2}} \qquad (86)$$

and,

$$P_L = \tan^{-1}\left[-\frac{RK\omega C}{R+K}\right] , \qquad (87)$$

and for the high pass filter,

$$|A|_H = \frac{RK\omega C}{\sqrt{(R+K)^2 + R^2K^2\omega^2C^2}} , \qquad (88)$$

and

$$P_H = \tan^{-1}\left[\frac{R+K}{RK\omega C}\right] \qquad (89)$$

As long as the same value resistors and capacitors are used there is a 90 degree shift between the outputs of the low and high pass filters. It was convenient then to select R and C values such that at a particular frequency, the amplitude attenuation was the same in each filter. This was accomplished when,

$$R = \frac{1}{\omega C} = \frac{1}{2\pi fC} . \qquad (90)$$

The amplitude parts of both the low and high pass filters under the condition of equation (90) are then

$$|A|_H = |A|_L = \frac{K}{\sqrt{(R + K)^2 + K^2}} \qquad (110)$$

while the phase parts are

$$P_L = \tan^{-1}\left[-\frac{K}{R + K}\right], \qquad (111)$$

and

$$P_H = \tan^{-1}\left[\frac{R + K}{K}\right] \qquad (112)$$

The R and C values at each frequency set point are given in Table 9.

Polystyrene capacitors were used in values of 1, 0.1, and 0.01 microfarads. The R values were set on 10 turn 0.1 megohm potentiometers. Any additional resistance was provided by adding precision resistors in series with the potentiometers. These ±1% resistors were available in values of 0.1, 0.2, 0.5, and 1.0 megohms. The potentiometers were used as variable resistors and their set points are also given in Table 9.

The attenuation of the signals through the phase changing filters was calculated from equation (110) for the two values of input resistors used, 0.1 and 1.0 megohms. When this attenuation was normalized to one

TABLE 9

SET POINTS FOR PHASE SHIFTERS

f cycles per second	C micro-farads	R megohms	External Resistors 0.1 megohms	0.1 Megohm Potentiometers set point
0.1	1.0	1.5916	10 - 5	084
0.15	1.0	1.0610	10 - 0	390
0.2	1.0	0.7958	5 - 2	042
0.3	1.0	0.5305	5 - 0	695
0.4	1.0	0.3979	2 - 1	021
0.5	1.0	0.3183	2 - 1	817
0.6	1.0	0.2653	2 - 0	347
0.7	1.0	0.2274	2 - 0	726
0.8	1.0	0.1989	1 - 0	011
0.9	1.0	0.1768	1 - 0	232
1.0	1.0	0.1592	1 - 0	408
1.25	1.0	0.1273	1 - 0	727
1.5	1.0	0.1061	1 - 0	939
2.0	1.0	0.0796	0 - 0	204
2.5	1.0	0.0637	0 - 0	363
3.0	1.0	0.0530	0 - 0	470
4.0	1.0	0.0398	0 - 0	602
5.0	1.0	0.0318	0 - 0	682
6.0	1.0	0.0265	0 - 0	735
7.0	1.0	0.0227	0 - 0	773
8.0	1.0	0.0199	0 - 0	801
9.0	1.0	0.0177	0 - 0	823
10.0	1.0	0.0159	0 - 0	841
12.5	1.0	0.0127	0 - 0	873
15.0	1.0	0.0106	0 - 0	894
20.0	0.1	0.0796	0 - 0	204
25.0	0.1	0.0637	0 - 0	363
30.0	0.1	0.0530	0 - 0	470
40.0	0.1	0.0398	0 - 0	602
50.0	0.1	0.0318	0 - 0	682
60.0	0.1	0.0265	0 - 0	735
70.0	0.1	0.0227	0 - 0	773
80.0	0.1	0.0199	0 - 0	801
90.0	0.1	0.0177	0 - 0	823
100.0	0.1	0.0159	0 - 0	841
125.0	0.1	0.0127	0 - 0	873
150.0	0.1	0.0106	0 - 0	894
200.0	0.01	0.0796	0 - 0	204

for the complete isolation of the filter, i.e. for X very large, the reciprocal squared of the attenuation was the correction factor to be applied for the phase change filters. These correction factors are given in Table 10

The attenuation due to the high pass filter before multiplication was calculated from equation (88). The outputs of these filters were always fed into 1.0 megohm input resistors. Once again, the square of the reciprocal of this attenuation was the correction factor for the high pass filters. This correction factor is also given in Table 10 as well as the combined correction factor, (CF), which takes both phase shifter attenuation and high pass filter attenuation into account.

Once again it is noted that these corrections were unnecessary in the measurement of the quantity $R_{12}(\omega)$, but were used when cross-power or power spectra were measured with the analyzer.

TABLE 10

CORRECTION FACTORS FOR FILTERS

f cycles per second	Correction Factor for Phase Changer K=1.0 megohm	Correction Factor for Phase Changer K=0.1 megohm	Correction Factor for High Pass Filter	Combined System Correction Factor (CF) K=1.0 megohm	Combined System Correction Factor (CF) K=0.1 megohm
0.1	3.86	144.0	3.59	13.8	517.0
0.15	2.63	68.2	2.08	5.46	142.0
0.2	2.10	61.9	1.64	3.55	102.0
0.3	1.66	20.3	1.30	2.16	26.4
0.4	1.49	13.0	1.15	1.71	14.9
0.5	1.36	9.20	1.10	1.50	10.1
0.6	1.29	7.03	1.07	1.38	7.52
0.7	1.25	5.86	1.05	1.31	6.15
0.8	1.22	4.94	1.04	1.27	5.12
0.9	1.19	4.37	1.03	1.23	4.50
1.0	1.17	4.16	1.02	1.19	4.25
1.25	1.14	3.10	1.02	1.16	3.16
1.5	1.11	2.62	1.01	1.12	2.65
2.0	1.08	2.10	1.01	1.09	2.12
2.5	1.05	1.82	1.00	1.05	1.82
3.0	1.05	1.66	1.00	1.05	1.66
4.0	1.04	1.46	1.00	1.04	1.46
5.0	1.04	1.37	1.00	1.04	1.37
6.0	1.02	1.30	1.00	1.02	1.30
7.0	1.02	1.26	1.00	1.02	1.26
8.0	1.02	1.21	1.00	1.02	1.21
9.0	1.01	1.19	1.00	1.01	1.19
10.0	1.01	1.17	1.00	1.01	1.17
12.5	1.01	1.12	1.00	1.01	1.12
15.0	1.01	1.10	1.00	1.01	1.10
20.0	1.08	2.10	1.00	1.08	2.10
25.0	1.05	1.82	1.00	1.05	1.82
30.0	1.05	1.66	1.00	1.05	1.66
40.0	1.04	1.46	1.00	1.04	1.46
50.0	1.04	1.37	1.00	1.04	1.37
60.0	1.02	1.30	1.00	1.02	1.30
70.0	1.02	1.26	1.00	1.02	1.26
80.0	1.02	1.21	1.00	1.02	1.21
90.0	1.01	1.19	1.00	1.01	1.19
100.0	1.01	1.17	1.00	1.01	1.17
125.0	1.01	1.12	1.00	1.01	1.12
150.0	1.01	1.10	1.00	1.01	1.10
200.0	1.08	2.10	1.00	1.08	2.10

APPENDIX C

OPERATION OF CROSS-POWER SPECTRUM ANALYZER

The measurement of the quantity $R_{12}(\omega)$, defined by equation (69), requires that three voltages be measured on the cross-power spectrum analyzer; V, related to the power spectrum of the output of the externally disturbed region of the reactor through equation (93), V_R, related to the real part of the cross-power spectrum between the outputs of the two regions of the reactor by equation (91), and V_I, related to the imaginary part of the cross-power spectrum between the outputs of the two regions of the reactor by equation (92).

Figure 9 is a schematic of the cross-power spectrum analyzer. The tape recorder and demodulators are included in the figure but were not needed, of course, for "on line" data processing.

The first step in the processing of each data run was the amplification of the ac portions of the two signals from the demodulators (or the two signals directly in the case of "on line" processing) to about 10 volts peak to peak. A gain of about 25 was found to be sufficient for most runs. Once this gain was established it was used throughout the run.

The first step taken at each frequency point was to set the band pass filters and the R and C values of the phase shifters. The frequency set points on the band pass filters were determined by a previous calibration with a signal generator. The R and C values used were those as listed in Table 9 of Appendix B.

The most convenient way to measure the power spectrum of the output of the externally excited region of the reactor was to feed its signal into both channels of the analyzer. This procedure also afforded a check on the frequency settings of the band pass filters. The output of one band pass filter was fed to the vertical axis of a dual beam oscilloscope and the output of the other band pass filter to the horizontal axis of the oscilloscope. Since the input signals to the band pass filters were identical the Lissajous figure formed on the oscilloscope was a straight line. Any departure from a straight line presentation was corrected by a fine adjustment of the band pass filter settings.

The gain, M, of the amplifiers between the phase shifters and the high pass filters was then adjusted so that the signals had a strength from 100 to 200 volts peak to peak. Two potentiometers could be adjusted in each of the three signal paths All potentiometers were set with the null potentiometer. It was also possible to set the gain of the amplifiers at the output of the phase changers at either 1 or 10. M values of from 40 to 2500 were employed.

The time constant of the integrating amplifiers was set from 0.0001 to 0.0003. Once again, the potentiometers used for these settings were set with the null potentiometer. It was desirable to select a time constant such that about 50 volts would be collected across the integrator during the three minute integration time.

The measurement of the power spectrum of the externally disturbed region of the reactor was performed by feeding its signal, $f_1(t)$, into both channels of the analyzer, making the setting described above, turning the analog computer to operate for three minutes then switching it to hold, and reading the voltage on the integrating amplifier with the null potentiometer. The voltage V, related to the power spectrum appeared across the integrator ordinarily giving the real part voltage during cross-power spectrum analysis.

After V was measured, the signal representing the output of the other region of the reactor, $f_2(t)$, was used in the second channel of the analyzer instead of $f_1(t)$. Then at each frequency set point, the same settings and procedures were used to measure the voltages V_R and V_I as were used to measure the voltage V.

LIST OF REFERENCES

1. E. P. Wigner, Use of the Pile Oscillator for the Measurement of Pile Constants, CP-3066, June 23, 1945.

2. A. F. Henry, The Application of Reactor Kinetics to the Analysis of Experiments, Nuclear Sci. and Eng., 3, 52-70 (1959).

3. F. deHoffman, Intensity Fluctuations of a Neutron Chain Reactor, MDDC-382, LADA-256 (declassified October 7, 1946).

4. W. K. Luckow, "The Evaluation of Nuclear Reactor Parameters from Measurements of Neutron Statistics," Ph.D. Dissertation, University of Michigan, 1958.

5. R. W. Albrecht, The Measurement of Dynamic Nuclear Reactor Parameters by Methods of Stochastic Processes, Trans. Am. Nuclear Soc., 4, 2 (1961) pp. 311-312.

6. C. Velez, 'Autocorrelation Functions of Counting Rate in Nuclear Reactors and Their Application to the Design of Reactor Control Instrumentation,' Ph.D. Dissertation, University of Michigan, 1959.

   A less complete description of this work is found in

   C. Velez, Autocorrelation Functions of Counting Rate in Nuclear Reactors, Nuclear Sci. and Eng., 6, 414-419 (1959).

7. M. N. Moore, The Determination of Reactor Transfer Functions from Measurements at Steady Operation, Nuclear Sci. and Eng., 3, 387-394 (1958).

8. M. N. Moore, The Power Noise Transfer Function of a Reactor, Nuclear Sci. and Eng., 6, 448-452 (1959).

9. C. E. Cohn, Determination of Reactor Kinetic Parameters by Pile Noise Analysis, Nuclear Sci. and Eng., 5, 331-335 (1959).

10. C. W. Griffin and J. G. Lundholm, Measurement of the SRE and KEWB Prompt Neutron Lifetime Using Random Noise and Reactor Oscillation Techniques, NAA-SR-3765, Oct. 1959.

11. C. E. Cohn, A Simplified Theory of Pile Noise, *Nuclear Sci. and Eng.*, *7*, 472-475 (1960).

12. E. F. Bennett, The Rice Formulation of Pile Noise, *Nuclear Sci. and Eng.*, *8*, 53-61 (1960).

13. S. O. Rice, Mathematical Analysis of Random Noise, from N. Wax, "Selected Papers on Noise and Stochastic Processes," pp. 133-294, Dover, New York, 1954.

14. C. W. Griffin and R. L. Randall, Reactor Power Spectrum Measurements, *Trans. Am. Nuclear Soc.*, *5*, 1 (1962) pp. 174-175.

15. J. D. Balcomb, "A Crosscorrelation Method for Measuring the Impulse Response of Reactor Systems," Ph.D. Dissertation, Massachusetts Institute of Technology, June 1961.

    A less complete description of this work is given in

    J. D. Balcomb, *et al.*, A Crosscorrelation Method for Measuring the Impulse Response of Reactor Systems, *Nuclear Sci. and Eng.*, *11*, 159-166 (1961).

16. V. Rajagopal, "Experimental Study of Nuclear Reactor Internal Noise and Transfer Functions Using Random Reactivity Variations and Correlation Analysis," Ph.D. Dissertation, Rensselaer Polytechnic Institute, Troy, N. Y., 1960.

    A less complete description of this work is given in

    V. Rajagopal, Determination of Reactor Transfer Functions by Statistical Correlation Methods, *Nuclear Sci. and Eng.*, *12*, 218-224 (1962).

17. G. C. Baldwin, Kinetics of a Reactor Composed of Two Loosely Coupled Cores, *Nuclear Sci. and Eng.*, *6*, 320-327 (1959).

18. M. A. Schultz, "Control of Nuclear Reactors and Power Plants," 2nd ed., McGraw-Hill, New York, 1961.

19. Y. W. Lee, "Statistical Theory of Communication," John Wiley and Sons New York, 1960.

20. J. S. Bendat, "Principles and Applications of Random Noise Theory," John Wiley and Sons, New York, 1958.

21. C. E. Cohn, Reflected-Reactor Kinetics, Nuclear Sci. and Eng., 13, 12-17 (1962)

22. A. M. Weinberg and E. P. Wigner, "The Physical Theory of Neutron Chain Reactors," University of Chicago Press, Chicago, 1958.

23. J. M. Duncan, "University of Florida Training Reactor Hazards Summary Report," Florida Engineering and Industrial Experiment Station, Gainesville, October 1958.

24. R. B. Blackman and J. W. Tukey, "The Measurement of Power Spectra," Dover, New York, 1958, p. 58.

25. J. Millman and H. Taub, "Pulse and Digital Circuits," McGraw-Hill, New York, 1956, pp. 28-46.

26. Bennett and Fulton, The Generation and Measurement of Low Frequency Random Noise, Journal of Applied Physics, 22, 1187-1191, 1951.

27. R. W. Badgley, "Power Spectral Density of the University of Florida Training Reactor Operating in the Subcritical Region," M.S. Thesis, University of Florida, 1962.

28. R. H. Chastain, "Transfer Function of the University of Florida Training Reactor," M.S. Thesis, University of Florida, Gainesville, Florida, 1961.

29. C. A. Thompson, "Neutron Flux Calculations for a Graphite Moderated Twenty Per Cent Enriched Reactor," M.S. Thesis, University of Florida, Gainesville, Florida, 1961.

BIOGRAPHICAL SKETCH

Allen Ross Boynton was born in Lexington Kentucky, on June 16, 1936. In June, 1953, he was graduated from Owensboro Senior High School, Owensboro, Kentucky. In June, 1957, he received the degree of Bachelor of Science in Mechanical Engineering, with distinction, from Purdue University. He was awarded an Atomic Energy Commission Fellowship in September, 1957, and received the degree of Master of Science in Engineering from Purdue University in August, 1958. In September, 1958, he was admitted to the University's Graduate School. While pursuing his graduate studies, he held positions as Graduate Assistant and as the Chief Operator of the University of Florida Training Reactor.

Allen Ross Boynton is married to the former Carol Sue Baringer of Gainesville, Florida. He is a member of Tau Beta Pi, Pi Tau Sigma, and the American Nuclear Society.

This dissertation was prepared under the direction of the chairman of the candidate's supervisory committee and has been approved by all members of that committee. It was submitted to the Dean of the College of Engineering and to the Graduate Council, and was approved as partial fulfillment of the requirements for the degree of Doctor of Philosophy.

December, 1962

Joseph Weil

Dean, College of Engineering

Dean, Graduate School

Supervisory Committee:

Robert E Uhrig

Chairman

C. B. Smith

John C Reed

G R Dalton